ACS NANO

www.acsnano.org

ARTICLE

# 杂原子掺杂闪蒸石墨烯
# Heteroatom-Doped Flash Graphene

Weiyin Chen,[#] Chang Ge,[#] John Tianci Li, Jacob L. Beckham, Zhe Yuan, Kevin M. Wyss, Paul A. Advincula, Lucas Eddy, Carter Kittrell, Jinhang Chen, Duy Xuan Luong, Robert A. Carter, and James M. Tour*

Cite This: https://doi.org/10.1021/acsnano.2c01136

Read Online

ACCESS | Metrics & More | Article Recommendations | Supporting Information

摘要：杂原子掺杂可以有效地调整本征二维材料的局部结构和电子态，并赋予其改进的光学、电学和机械性能。

**ABSTRACT:** Heteroatom doping can effectively tailor the local structures and electronic states of intrinsic two-dimensional materials, and endow them with modified optical, electrical, and mechanical properties. 最近的研究表明，通过一些后处理(包括固态和溶剂热方法)从氧化石墨烯及其衍生物制备掺杂石墨烯是可行的，但它们需要反应性和苛刻的试剂。 Recent studies have shown the feasibility of preparing doped graphene from graphene oxide and its derivatives via some post-treatments, including solid-state and solvothermal methods, but they require reactive and harsh reagents. 然而，通过自下而上的方法直接合成大量高纯度的各种杂原子掺杂石墨烯仍然具有挑战性。 However, direct synthesis of various heteroatom-doped graphene in larger quantities and high purity through bottom-up methods remains challenging. 在这里，我们报道了通过快速焦耳加热(FJH)无催化剂和无溶剂直接合成掺杂各种杂原子的石墨烯。 Here, we report catalyst-free and solvent-free direct synthesis of graphene doped with various heteroatoms in bulk via flash Joule heating (FJH). 通过毫秒闪蒸合成了七种杂原子掺杂的闪蒸石墨烯，包括单元素掺杂的闪蒸石墨烯(硼、氮、氧、磷、硫)、双元素共掺杂的闪蒸石墨烯(硼和氮)以及三元素共掺杂的闪蒸石墨烯(硼、氮和硫)。 Seven types of heteroatom-doped flash graphene (FG) are synthesized through millisecond flashing, including single-element-doped FG (boron, nitrogen, oxygen, phosphorus, sulfur), two-element-*co*-doped FG (boron and nitrogen), as well as three-element-*co*-doped FG (boron, nitrogen, and sulfur). 使用多种低成本掺杂剂，例如单质、氧化物和有机化合物。 A variety of low-cost dopants, such as elements, oxides, and organic compounds are used. 杂原子掺杂FG的石墨烯质量高，与本征FG类似，该材料表现出涡轮层状、增加的层间距和优异的分散性。 The graphene quality of heteroatom-doped FG is high, and similar to intrinsic FG, the material exhibits turbostraticity, increased interlayer spacing, and superior dispersibility. 测试了不同杂原子掺杂FG的电化学氧还原反应，其中硫掺杂FG的性能最好。 Electrochemical oxygen reduction reaction of different heteroatom-doped FG is tested, and sulfur-doped FG shows the best performance. 锂金属电池测试表明，与铜或未掺杂FG相比，氮掺杂FG的成核过电位较小。 Lithium metal battery tests demonstrate that nitrogen-doped FG exhibits a smaller nucleation overpotential compared to Cu or undoped FG. 合成掺杂杂原子的FG合成的电能成本仅为1.2到1.5%。 The electrical energy cost for the synthesis of heteroatom-doped FG synthesis is only 1.2 to 10.7 kJ/g，这可以使FJH方法适用于低成本大规模生产掺杂杂原子的石墨烯。 10.7 kJ g$^{-1}$, which could render the FJH method suitable for low-cost mass production of heteroatom-doped graphene.

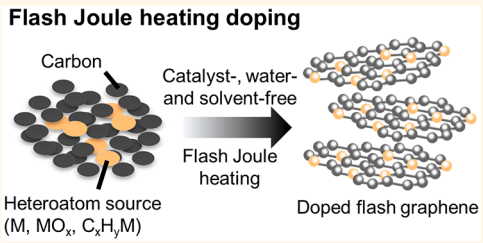


关键词：闪蒸焦耳加热、直接合成、闪蒸石墨烯、杂原子掺杂、无催化剂

**KEYWORDS:** *flash Joule heating, direct synthesis, flash graphene, heteroatom-doping, catalyst-free*

## INTRODUCTION

本征纳米材料的化学功能化已广泛用于调整局部结构和电子状态，从而极大地影响材料的光学、电学和机械性能。 Chemical functionalization of intrinsic nanomaterials has been widely used to tailor the local structures and electronic states, thereby greatly affecting the materials' optical, electrical, and mechanical properties. 实现化学修饰的传统方法包括将各种杂原子、特定官能团、甚至其他分子引入固有晶格。 Traditional methods to achieve chemical modification involve the introduction of various heteroatoms,[3,5] specific functional groups,[1,6] or even other molecules[7] into the intrinsic lattice. 杂原子掺杂是一种最基本但高效的改性方法，它包括用其他元素取代原始成分。 Heteroatom doping, which consists of substituting the original components with other elements, is the most basic yet highly effective modification.[5,8] 对于石墨烯，可以引入许多不同的掺杂剂，包括氮、硫、氧、硼、磷和一些金属原子。 For graphene, many different dopants can be introduced, including nitrogen, sulfur, oxygen, boron, phosphorus, and some metal atoms. 杂原子掺杂的石墨烯具有电催化性能，在传感应用中具有优越的性能，和与各种聚合物以及单个金属原子更强的相互作用。 Heteroatom-doped graphene has demonstrated electrocatalytic properties, superior performance in sensing applications,[5] and stronger interactions with various polymers as well as single metal atoms.[10] 先前的研究主要集中在预制石墨烯晶格的化学功能化(后处理)，包括球磨、氧化石墨烯(GO)的热退火、等离子体处理和光化学反应。 Previous research has focused on the chemical functionalization of preformed graphene lattice (post-treatment), including ball milling,[5] thermal annealing of graphene oxide (GO),[13,14] plasma treatment, and photochemical reactions. 球磨法和等离子体法是合成杂原子掺杂石墨烯的简单且可扩展的方法，但掺杂通常局限于边缘或其他缺陷。 Ball milling and plasma methods are simple and scalable routes to synthesize heteroatom-doped graphene, but the doping is usually limited at the edges or other defects.[5,15,16] 热退火方法不仅需要GO作为在剧烈氧化下合成的前驱体，还需要延长高温以部分恢复sp2碳网络。 Thermal annealing method not only needs GO as the precursor, which is synthesized under harsh oxidation, but also requires extended high temperature to partially recover the sp$^2$ carbon network.[13,14] 这些自上而下插入石墨烯通常会导致石墨烯质量的不可逆退化，这些步骤可能会有问题，因为它们会导致过量供应反应剂(如KMnO4和BCl3)不可避免地产生杂质。大多数自底向上直接合成掺杂杂原子的石墨烯可以通过化学气相沉积(CVD)或合成有机策略实现，但产品仅限于超微量，从μg到mg，而且它们通常含有催化金属杂质，如铬、钛和镍。 These top-down insertions into graphene usually cause irreversible degradation of graphene quality, and these procedures can be problematic since they result in inevitable impurities from the excessive supply of reactive agents such as $KMnO_4$ and $BCl_3$.[1,5] Most bottom-up direct synthesis of heteroatom-doped graphene can be achieved by chemical vapor deposition (CVD)[17] or synthetic organic strategies,[18] but the products are limited to ultrasmall amounts, from μg- to mg-scales, and they often suffer from catalytic metal impurities such as Cr, Ti, and Ni. 此外，可实现的异质掺杂石墨烯组合物的类型通常受到前体蒸汽压或溶解度的限制。 Furthermore, the types of heteroatom-doped graphene compositions achievable are often restricted by the vapor pressure or solubility of the precursors.[5]

**Received:** February 2, 2022

**Accepted:** March 18, 2022

因此，从非晶碳源直接固相合成大量的异质掺杂石墨烯可以潜在地解决这些难题。
Therefore, the direct solid-phase synthesis of heteroatom-doped graphene in bulk quantities from amorphous carbon sources can potentially solve these dilemmas.

在这里，我们揭示了一种在1秒内通过超快和全固态无催化剂快速焦耳加热(FJH)方法合成异质掺杂石墨烯的一般路线。
Here, we disclose a general synthetic route to heteroatom-doped graphene by ultrafast and all-solid-state catalyst-free flash Joule heating (FJH) method within 1 s. 它不需要溶剂、催化剂和水。 It requires no solvent, no catalysts, and no water. 高能量密度的短电脉冲通过固体前体，在>10^5 K/s时将样品温度升高到>3500 K，然后在>10^4 K/s时快速冷却。 A short electrical pulse of high energy density is passed through the solid precursors, 七种重要的杂原子掺杂闪蒸石墨烯(FG)，包括单元素掺杂(B，N，O，P，S)、二元素共掺杂(B，N)和三元素共掺杂(B，N，S)FG，通过毫秒闪蒸与各种低成本源(包括元素、氧化物和有机化合物)制备。 which raises the sample temperature to >3500 K at >$10^{4}$ K $s^{-1}$ followed by rapid cooling at >$10^{4}$ K $s^{-1}$. Seven types of important heteroatom-doped flash graphene (FG), including single-element-doped (B, N, O, P, S), two-element-*co*-doped (B, N), and three-element-*co*-doped (B, N, S) FG are produced by millisecond flashing with various low-cost sources, including elements, oxides, and organic compounds. 这证明了FJH方法的多功能性。 This demonstrates the versatility of the FJH method. 选择这些掺杂剂是因为它们可以提供空气稳定的掺杂石墨烯产品。 These dopants were selected since they can afford air-stable doped graphene products. 光谱分析表明，杂原子掺杂FG具有良好的石墨烯质量和修饰的电子结构。 Spectroscopic analysis indicates that heteroatom-doped FG has good graphene quality and modified electronic structure. 此外，我们证明了在纳米尺度上精确控制尺寸分布以及直接使用掺杂杂原子的FG，而无需费力的纯化程序。 Moreover, we demonstrate the precise control of size distribution at the nanoscale and the direct usage of heteroatom-doped FG without laborious purification procedures. 研究了这些材料的分散性，并在电化学氧还原反应(ORR)和锂金属电池(LMB)组成中进行了测试。 The materials were studied for their dispersibility, and tested in electrochemical oxygen reduction reactions (ORR) and lithium metal battery (LMB) compositions. 此外，探索了杂原子掺杂FG的克级合成，以证明扩大其生产的可行性。 In addition, gram-scale synthesis of heteroatom-doped FG is explored to demonstrate the feasibility of scaling up its production.

结果和讨论
## RESULTS AND DISCUSSION

闪蒸焦耳加热直接合成掺杂杂原子的石墨烯。
**Direct Synthesis of Heteroatom-Doped Graphene by Flash Joule Heating.** 在典型的快速合成过程中，掺杂剂和导电炭黑的粉末混合物在两个配合良好的石墨垫片之间的厚壁聚合物管内被轻微压缩(图S1)。 In a typical flash synthesis process, the powdery mixture of dopants and conductive carbon black is slightly compressed inside a thick-walled polymer tube between two well-fitted graphite spacers (Figure S1). 聚合物管可以由聚四氟乙烯、聚(1,4-苯硫醚)或聚丙烯腈制成。 The polymer tube can be made from Teflon, poly(1,4-phenylene sulfide), or polyacrylonitrile. 电路中的电容器组连接到石墨垫片，用于在小于1秒的时间内向反应物提供电热能。 The capacitor banks in the circuit are connected to graphite spacers and are used to provide electrothermal energy to the reactants in <1 s. 与我们之前的出版物中使用的松软铜棉电极相比，厚壁聚合物管和良好安装的石墨间隔大大减少了杂原子的损失，并促进了杂原子掺杂石墨烯的形成。 Compared to fluffy copper wool-made electrodes used in our previous publications, thick-walled polymer tubes and well-fitted graphite spacers greatly decrease the loss of heteroatoms and facilitate the formation of the heteroatom-doped graphene. 表1列出了详细的闪蒸参数。不同的掺杂剂可以用作前体，包括单质(M)、氧化物($MO_x$)和有机化合物($C_xH_yM$)(图1a)。 The detailed flash parameters are listed in Table 1. Different dopants can be used as precursors, including elements (M), oxides ($MO_x$), and organic compounds ($C_xH_yM$) (Figure 1a). 在电压为110 V、样品电阻为1.0的典型FJH合成过程中，通过样品的电流在100 ms放电时间内达到60 A(图S2)。 During a typical FJH synthesis process with a voltage of 110 V and a sample resistance of ~1.0 Ω, the current passing through the sample reaches ~60 A within ~100 ms discharge time (Figure S2). 以掺氮FG(N-FG)为例，总电能为6.6 kJ/g(表S1)。 Take nitrogen-doped FG (N-FG) as an example, the total amount of electrical energy is 6.6 kJ $g^{-1}$ (Table S1). 通过拟合FJH过程中的黑体辐射光谱来测量温度(图S3)。 The temperature is measured by fitting the blackbody radiation spectra during the FJH process (Figure S3). 瞬态最高温度在2.0×10^5 K/s时达到3500 K，随后55 ms后的超快冷却速率估计为1.8×10^4 K/s(图1b)，这有助于形成具有较大层间间距的涡轮层结构。 The transient highest temperature reaches ~3500 K at ~$2.0 \times 10^{5}$ K $s^{-1}$ and subsequent ultrafast cooling rate after ~55 ms is estimated as ~$1.8 \times 10^{4}$ K $s^{-1}$ (Figure 1b), which facilitates the formation of turbostratic structures with larger interlayer spacings. 这种超快冷却不允许AB堆叠石墨烯发生，这有助于在溶剂中分散，如以前的出版物所示。 This ultrafast cooling does not permit AB-stacked graphene to occur, which facilitates dispersion in solvents as seen in the previous publications. 瞬态超高温挥发杂原子成分，并增强这些前体蒸汽与非晶碳源之间的均相反应，以形成掺杂石墨结构 The transient ultrahigh temperature volatilizes the heteroatom components and enhances the homogeneous reactions between these precursor vapors and the amorphous carbon source to form the doped graphitic

表1。不同系统的闪蒸参数
**Table 1. Flash Parameters for Different Systems**

| | FG | N-FG | B-FG | O-FG |
|---|---|---|---|---|
| 反应物 reactant | CB | 三聚氰胺+炭黑 melamine + CB (75 wt %) | 硼酸+炭黑 boric acid + CB (80 wt %) | 蔗糖+炭黑 sucrose + CB (60 wt %) |
| 样品质量 sample mass (mg) | 30 | 40 | 40 | 40 |
| 样品电阻 sample resistance (Ω) | ~0.7 | ~0.9 | ~2.0 | ~5.0 |
| 放电电压 discharge voltage (V) | 110 | 110 | 110 | 120 |
| 闪蒸持续时间 flash duration (ms) | 100 | 100 | 100 | 200 |
| 闪蒸重复 flash repetitions | 1 flash | 1 flash | 1 flash | 3 flashes |
| 总电容 total capacitance (mF) | 60 | 60 | 60 | 60 |
| 腔室压力 chamber pressure | Ar (~1 atm) | Ar (~1 atm) | Ar (~1 atm) | Ar (~1 atm) |

| | P-FG | S-FG | B,N-FG |
|---|---|---|---|
| 反应物 reactant | 红磷+炭黑 red phosphorus + CB (90 wt %) | 聚苯硫醚+炭黑 PPS + CB (50 wt %) | 硼：三聚氰胺 boron:melamine:CB (2:5:23)[a] |
| 样品质量 sample mass (mg) | 25 | 40 | 40 |
| 样品电阻 sample resistance (Ω) | ~1.5 | ~1.0 | ~3.0 |
| 放电电压 discharge voltage (V) | 120 | 120 | 110 |
| 闪蒸持续时间 flash duration (ms) | 200 | 100 | 50 |
| 闪蒸重复 flash repetitions | 3 flashes | 1 flash | 1 flash |
| 总电容 total capacitance (mF) | 60 | 60 | 60 |
| 腔室压力 chamber pressure | Ar (~1 atm) | Ar (~1 atm) | Ar (~1 atm) |

| | B,N,S-FG | N-FG-L1 | N-FG-L2 |
|---|---|---|---|
| 反应物 reactant | 硼：三聚氰胺：聚苯硫醚：炭黑 boron:melamine:PPS:CB (3:4:12:12)[a] | melamine + CB (75 wt %) | 三聚氰胺+炭黑三聚氰胺+炭黑 melamine + CB (75 wt %) |
| 样品质量 sample mass (mg) | 40 | 320 | 1000 |
| 样品电阻 sample resistance (Ω) | ~1.3 | ~1.0 | ~0.4 |
| 放电电压 discharge voltage (V) | 100 | 155 | 175 |
| 闪蒸持续时间 flash duration (ms) | 50 | 200 | VFD[b] |
| 闪蒸重复 flash repetitions | 1 flash | 1 flash | 1 flash |
| 总电容 total capacitance (mF) | 60 | 222 | 624 |
| 腔室压力 chamber pressure | Ar (~1 atm) | Ar (~1 atm) | Air (~1 atm) |

[a]此处使用质量比。 Mass ratios are used here. [b]VFD指变频驱动，是一种通过改变电源频率和持续时间来驱动电气开关的控制器。 VFD means "variable frequency drive", which is a type of controller that drives an electric switch by varying the frequencies and durations of its power supply. 在这里，使用10%占空比1s，然后使用20%占空比5s。 Here, 10% duty cycle for 1s followed by 20% duty cycle for 5 s was used.

因此，FJH工艺不需要使用额外的催化剂或过量的反应剂，从而避免了重复的后净化过程，如渗析。 Therefore, FJH process does not require the use of extra catalysts or excessive reactive agents, which avoids redundant postpurification procedures, such as dialysis.[12] 相反，传统的后处理掺杂方法需要(i)GO作为碳源，(ii)气相或液相杂原子源，以及(iii)长达12小时的反应时间 In contrast, traditional post-treatment doping methods require (i) GO as the carbon source, (ii) gas- or solution-phase heteroatom sources, and (iii) long reaction time up to 12 h


https://doi.org/10.1021/acsnano.2c01136
ACS Nano XXXX, XXX, XXX−XXX

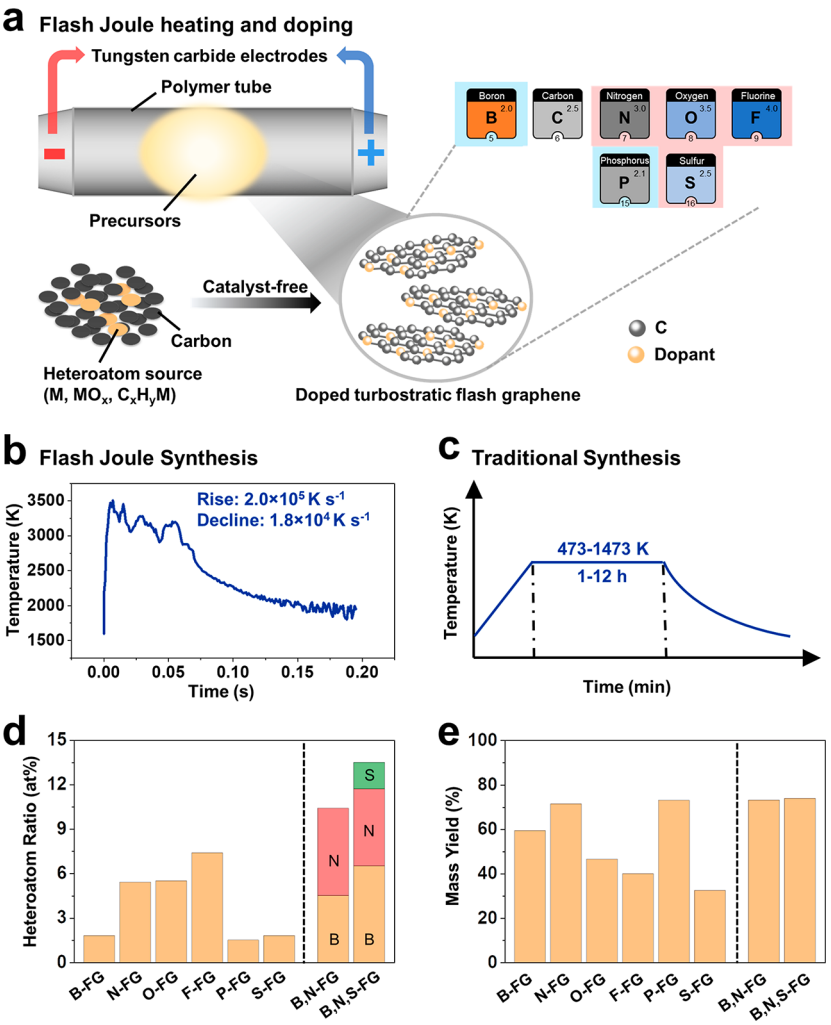


图1、闪蒸焦耳加热直接合成掺杂杂原子的石墨烯。(a)通过闪蒸焦耳加热合成杂原子掺杂涡轮层石墨烯的示意图。

**Figure 1. Direct synthesis of heteroatom-doped graphene by flash Joule heating. (a) Schematics of the synthesis of heteroatom-doped turbostratic graphene via flash Joule heating. (b) The real time temperature measurement during direct FJH synthesis of doped flash graphene. (c) Representative temperature profile of common procedures for the post-treatment synthesis of doped AB-stacked graphene, such as that from GO plus solid or gaseous heteroatom sources. (d) Heteroatom ratios and (e) mass yields for different heteroatom-doped flash graphene.**

(b)掺杂闪蒸石墨烯直接FJH合成过程中的实时温度测量。(c)掺杂AB堆叠石墨烯的后处理合成常用程序的代表性温度分布，例如来自GO+固体或气体杂原子源的程序。(d)不同杂原子掺杂的闪蒸石墨烯的杂原子比和(e)质量产率。

(图1c)。延长反应时间导致形成杂原子掺杂AB堆叠石墨烯，其比涡轮层石墨烯更难剥离。(Figure 1c). The extended reaction time leads to the formation of heteroatom-doped AB-stacked graphene,[1] which is harder to exfoliate than turbostratic graphene.[19]

对于单一类型的掺杂，合成的FG可以达到高达7.4%的杂原子比，对于多杂原子共掺杂，总杂原子比>10%，包括硼和氮(B，N-FG)以及硼、氮和硫(B，N，S-FG)，这表明了FJH工艺的广泛适用性(图1d)。The as-synthesized FG can reach a heteroatom ratio up to 7.4% for a single type dopant and a total heteroatom ratio >10% for multiple heteroatom codoping, including boron and nitrogen (B,N-FG) and boron, nitrogen, and sulfur (B,N,S-FG), demonstrating the broad applicability of the FJH process (Figure 1d). The FJH synthesis takes place in milliseconds within a thick-walled polymer tube with tightly fitting graphite spacers to minimize volatilization of the dopants. This enables a high mass conversion reaction yield up to 74% (Figure 1e).

FJH合成在厚壁聚合物管内以毫秒为单位进行，该厚壁聚合物管具有紧密贴合的石墨间隔物，以最小化掺杂剂的挥发。这使得高质量转化反应产率高达74%(图1e)。

**Characterization of Nitrogen-Doped Flash Graphene.** 氮掺杂闪蒸石墨烯的表征。我们首先研究了氮掺杂石墨烯，因为它是一种有效的电催化剂。We first explore the nitrogen-doped graphene, since it has been reported to be an effective electrocatalyst.[20,21] The incorporation of nitrogen into the honeycomb lattice of graphene can be diverse in its substitutional orientations, including pyridinic N, pyrrolic N, graphitic N, and nitrogen oxides (Figure 2a). These N-doped sites change the local symmetry along with electronic structure, and can behave as active sites for various electrochemical and electronic applications. Melamine ($C_3H_6N_6$) was our chosen dopant owing to its high nitrogen

氮在石墨烯蜂窝晶格中的掺入可以在其取代方向上不同，包括吡啶氮、吡咯氮、石墨氮和氮氧化物(图2a)。这些N掺杂位点随着电子结构的变化而改变局部对称性，并且可以作为各种电化学和电子应用的活性位点。三聚氰胺(C3H6N6)是我们选择的掺杂剂，因为它的氮含量高67 wt%的比例。

ratio of ~67 wt %. The as-synthesized N-FG has good graphene quality with N doping. The average Raman spectrum is collected from 100 sampling points and the standard deviation is <5%, which reflects the high homogeneity of the N-FG (Figure 2b). High D peak (~1339 cm$^{-1}$, breathing mode of sp$^2$-carbon atoms in rings), G peak (~1570 cm$^{-1}$, bonds stretching of all pairs of sp$^2$-carbon atoms in rings), and 2D peak (~2672 cm$^{-1}$, second order zone boundary phonons in graphene)[24] can be observed simultaneously and the 2D/G and D/G intensity ratios are ~0.84 and ~0.65, respectively, indicating abundant N-doped substitutional defect sites.[26,27] In contrast, intrinsic FG has a low $I_D/I_G$ < 0.05 and a high $I_{2D}/I_G$ ~ 1.95. The high-resolution Raman spectrum shows the existence of $TS_1$ (~1873 cm$^{-1}$) and $TS_2$ (~2018 cm$^{-1}$) peaks, and the absence of M peak (~1750 cm$^{-1}$) (Figure S4), substantiating the turbostratic oriented stacking of N-FG.[19,28] High-resolution Auger spectroscopy enables quantification of the D-parameter, which measures the energy separation between maxima and minima in differentiated C KLL spectrum. The D-parameter of N-FG is 22.4 eV and is close to graphene (Figure S5). The X-ray diffraction (XRD) result reflects a downshift of the (002) peak relative to parent

合成的N-FG在N掺杂下具有良好的石墨烯质量。从100个采样点收集平均拉曼光谱，标准偏差<5%，这反映了N-FG的高度均匀性(图2b)。可以同时观察到高D峰(1339 cm-1，环中sp2碳原子的呼吸模式)、G峰(1570 cm-1，环中所有sp2碳原子对的键拉伸)和2D峰(2672 cm-1，石墨烯中的二阶区域边界声子)，2D/G和D/G强度比分别为0.84和0.65，表明存在丰富的N掺杂取代缺陷位。相反，固有FG具有低ID/IG<0.05和高I2D/IG~1.95。高分辨率拉曼光谱显示存在TS1(1873 cm-1)和TS2(2018 cm-1)峰，并且没有M峰(1750 cm-1)(图S4)，证实了N-FG的涡轮层定向堆叠。高分辨率俄歇光谱能够量化D参数，D参数测量微分C KLL光谱中最大值和最小值之间的能量分离。N-FG的D参数为22.4 eV，接近石墨烯(图S5)。X射线衍射(XRD)结果反映了(002)峰相对于母原料的下移


https://doi.org/10.1021/acsnano.2c01136
ACS Nano XXXX, XXX, XXX−XXX

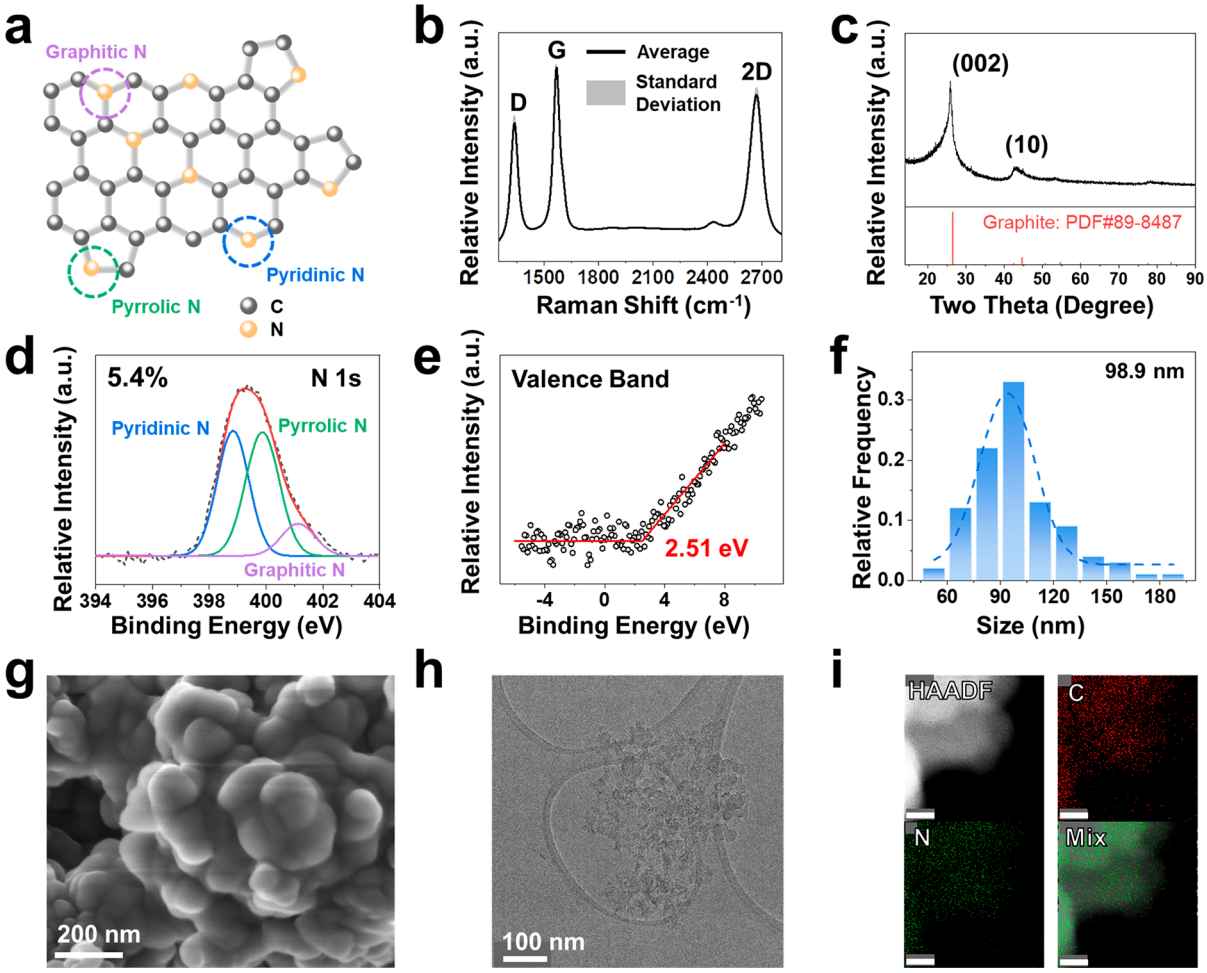


图2:氮掺杂闪蒸石墨烯的表征。(a)氮掺杂闪蒸石墨烯示意图。(b)氮掺杂闪蒸石墨烯的统计拉曼光谱。

**Figure 2. Characterization of nitrogen-doped flash graphene. (a) Schematic of nitrogen-doped flash graphene. (b) Statistic Raman spectrum of the nitrogen-doped flash graphene. The black line and the gray shadow represent the average value and the standard deviation of 100 sampling points, respectively. (c) XRD result of nitrogen-doped flash graphene (Powder Diffraction File 89-8487, Graphite). (d) High-resolution N 1s spectrum of nitrogen-doped flash graphene. (e) Valence band XPS spectrum of nitrogen-doped flash graphene. (f) The SEM-determined sheet size distribution of nitrogen-doped flash graphene determined over 100 nanoparticles. (g) Characteristic SEM and (h) TEM images of nitrogen-doped flash graphene. (i) HAADF-STEM image and corresponding elemental mapping results of nitrogen-doped flash graphene. The scale bars are 20 nm.**

黑线和灰色阴影分别表示100个采样点的平均值和标准差。(c)氮掺杂闪蒸石墨烯的XRD结果(粉末衍射文件89-8487，石墨)。(d)氮掺杂闪蒸石墨烯的高分辨率N 1s光谱。(e)氮掺杂闪蒸石墨烯的价带XPS光谱。(f)SEM测定了100多个纳米颗粒中氮掺杂闪蒸石墨烯的薄片尺寸分布。(g)氮掺杂闪蒸石墨烯的特征SEM和(h)TEM图像。(i)氮掺杂闪蒸石墨烯的HAADF-STEM图像和相应的元素映射结果。比例尺为20 nm。

石墨烯为25.9度，这表明层间间距扩大了2.7%(图2c)。

graphene to ~25.9 degree, which indicates the expansion of interlayer spacing by ~2.7% (Figure 2c). The general (100) and (101) reflections cannot be observed, and the asymmetric shape of the (10) reflection, which has a pronounced tailing effect on the high Bragg angle side, can be seen. These results support the absence of an ordered stacking of basal planes, and the existence of turbostratic structure. Since the carbon source is carbon black, N-FG and the other heteroatom-doped FG belong to the nongraphitizable carbons. Unlike the graphitizable carbon (also known as soft carbons), which could be directly transformed into crystalline graphite when they were heated to the temperature up to 3000 °C, typical nongraphitizable carbons (also known as hard carbons) could not be thermally transformed into graphite at this temperature. Since graphite is the thermodynamically most stable form of carbon, our previous study found that the merging of graphene sheets and the formation of AB-stacked layers can happen if the flash duration is increased to several seconds.[28]

无法观察到一般(100)和(101)衍射，并且可以看到(10)反射的不对称形状，其在高布拉格角侧具有明显的拖尾效应。这些结果支持了基面没有有序堆叠，以及涡轮层结构的存在。由于碳源为炭黑，N-FG和其他掺杂杂原子的FG属于难石墨化碳。与易石墨化碳(也称为软碳)不同，可石墨化碳在加热到3000 ° C时可以直接转化为晶体石墨，典型的难石墨化碳(也称为硬碳)在此温度下不能热转化为石墨。由于石墨是热力学上最稳定的碳形式，我们之前的研究发现，如果闪蒸持续时间增加到几秒，石墨烯片的合并和AB堆叠层的形成可能会发生。

N-FG的表面积为303 m2/g，丰富的孔径<10 nm(图S6)。

The surface area of N-FG is 303 $m^2 g^{-1}$ with abundant pore sizes <10 nm (Figure S6). N-FG has two types of the pores, closed pores, and open pores. The term of closed and open depends on the location and size of the pores into which a probe fluid (gas or liquid) can diffuse. The open porosity and the closed porosity are 0.54 and 0.11, respectively.

N-FG有两种类型的孔，封闭孔和开放孔。封闭和开放的术语取决于孔的位置和大小测试流体(气体或液体)可能会扩散。其开放孔隙度和闭合孔隙度分别为0.54和0.11。

N doping is confirmed by X-ray photoelectron spectroscopy (XPS). The elemental ratio of N is ~5.4% (Figure S7), the majority of which is in the form of pyridinic N (~398.7 eV) and pyrrolic N (~399.8 eV), with no indication of N-oxides (Figure 2d, Table S2). The ratio of pyridinic N and graphitic N reaches ~4.31. These pyridinic N atoms have unpaired electron spin density and exhibit strong interactions with some species, like metal atoms, which is useful in potential applications in electrocatalysts or metal electrodeposition.[10,25]

氮掺杂由X射线光电子能谱(XPS)证实。氮的元素比为5.4%(图S7)，其中大多数以吡啶氮(398.7 eV)和吡咯氮(399.8 eV)的形式存在，没有氮氧化物的迹象(图2d，表S2)。吡啶氮和石墨氮的比率达到~4.31。这些吡啶氮原子具有未配对的电子自旋密度，并与某些物种(如金属原子)表现出强烈的相互作用，这在电催化剂或金属电沉积中具有潜在的应用价值。

An appreciable valence band maximum (VBM) of −2.51 eV is measured for N-FG (Figure 2e). The N doping contents from 3 different batches are ~5.5%, 5.0%, and ~5.4%, which demonstrates the reliability of FJH method. Fourier transform infrared (FTIR) spectra of N-FG show the absence of melamine peaks and the signal of C—N and C═N stretching peaks in N-FG sample,[5] confirming the nitrogen doping during FJH process (Figure S8).

测量了N-FG的可观价带最大值(VBM)为2.51 eV(图2e)。3个不同批次的氮掺杂含量分别为5.5%、5.0%和5.4%，这证明了FJH方法的可靠性。N-FG的傅立叶变换红外光谱(FTIR)显示N-FG样品中不存在三聚氰胺峰以及C N和C N拉伸峰的信号，证实了FJH过程中的氮掺杂(图S8)。

The asymmetric broadening of the (002) diffraction peak reflects the nanosized feature of N-FG according to the Scherrer equation. The average size of 100 graphene sheets is

根据Scherrer方程，(002)衍射峰的不对称展宽反映了N-FG的纳米级特征。100个石墨烯片的平均尺寸为98.9 nm，


https://doi.org/10.1021/acsnano.2c01136
ACS Nano XXXX, XXX, XXX−XXX

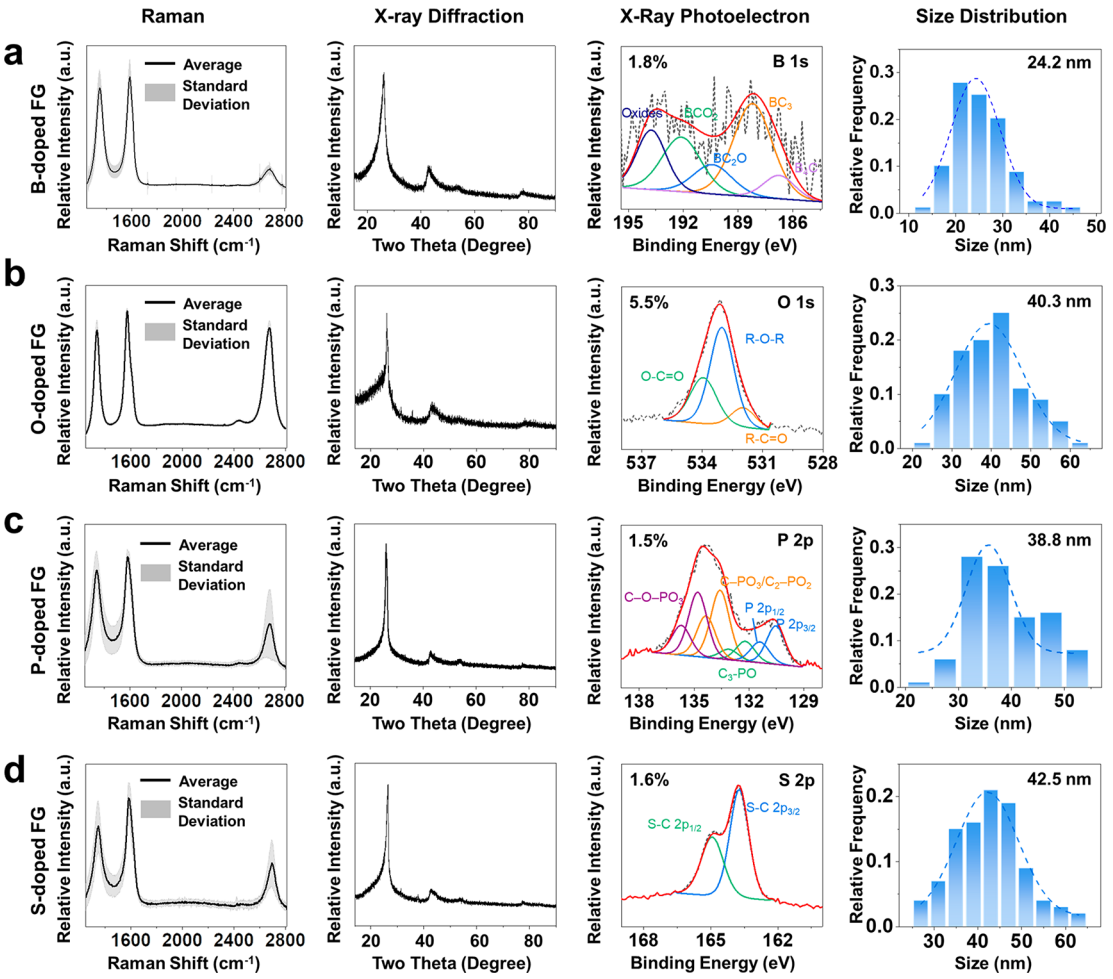


图3、杂原子掺杂闪蒸石墨烯的表征。表征结果，包括拉曼光谱(显示获得的平均光谱和超过100点的标准差)、XRD光谱、XPS结果(显示元素比率和键合状态)以及(a)掺硼闪蒸石墨烯、(b)掺氧闪蒸石墨烯、(c)掺磷闪蒸石墨烯和(d)掺硫闪蒸石墨烯的尺寸分布。

**Figure 3. Characterization of heteroatom-doped flash graphene. Characterization results, including Raman spectra (showing the average obtained spectra and standard deviations over 100 points), XRD spectra, XPS results (showing the elemental ratios and the bonding states), and the size distributions of (a) boron-doped flash graphene, (b) oxygen-doped flash graphene, (c) phosphorus-doped flash graphene, and (d) sulfur-doped flash graphene. The statistical Raman results are collected from 100 sampling points. High-resolution P 2p spectrum shows the splitting of each peak to $2p_{1/2}$ and $2p_{3/2}$ portions, which are denoted by the same color. The SEM-derived sheet size distribution results are obtained from at least 100 graphene sheets.**

从100个采样点收集统计拉曼结果。高分辨率P 2p光谱显示每个峰值分裂为2p1/2和2p3/2部分，用相同的颜色表示。从至少100个石墨烯薄片中获得了SEM衍生的薄片尺寸分布结果。

粒径分布较窄(图2f)，表明通过FJH合成可以精确控制石墨烯薄片的粒径，98.9 nm and the size distribution is narrow (Figure 2f), demonstrating the precise control of graphene flake size without obvious aggregation by FJH synthesis. The scanning electron microscopy (SEM) images show that N-FG is comprised of many nanocrystals (Figure 2g, Figure S9), and it is morphologically different from the undoped sheet-like FG, which usually has a lateral size up to several micrometers.[19,28] Transmission electron microscopy (TEM) confirms the existence of nanoparticles and high-resolution TEM (HR-TEM) images show the presence of lattice fringes along with jagged structures (Figure 2h, Figure S10). Energy-dispersive spectroscopy (EDS) shows the existence of N-doping (Figure S11). Scanning TEM (STEM) and corresponding elemental mapping demonstrate the homogeneous distribution of the N doping by FJH synthesis (Figure 2i).

而没有明显的聚集。扫描电子显微镜(SEM)图像显示，N-FG由许多纳米晶体组成(图2g、图S9)，其形态不同于未掺杂片状FG，后者通常具有高达数微米的横向尺寸。透射电子显微镜(TEM)证实了纳米颗粒的存在，高分辨率TEM(HR-TEM)图像显示存在晶格条纹和锯齿结构(图2h，图S10)。能量色散光谱(EDS)显示了N掺杂的存在(图S11)。扫描TEM(STEM)和相应的元素映射证明了FJH合成中N掺杂的均匀分布(图2i)。

FJH法合成杂原子掺杂闪蒸石墨烯

## FJH Synthesis of Heteroatom-Doped Flash Graphene.

证明了FJH合成的多功能性，并制备了五种不同的杂原子掺杂FG，包括硼、氮、氧、磷和硫掺杂FG(图1a)。The versatility of FJH synthesis is demonstrated and five distinct heteroatom-doped FG, including boron, nitrogen, oxygen, phosphorus, and sulfur-doped FG, are prepared (Figure 1a). The sealed polymer tubes prevent the dissipation of carbon and dopants, and a high mass conversion reaction yield (>70%) can be achieved as shown in Figure 1e. These heteroatoms have different atomic radii (50−100 pm) compared to carbon (70 pm) (Figure S12). Therefore, there is some lattice mismatch in heteroatom-doped graphene, and the formation of substitutional solid solutions are limited to certain feasible ranges without the destruction of the graphitic structure. The electronegativities of these heteroatoms (2.0−4.0) are distinct from that of carbon (2.5), and thus the intrinsic electronic structure of graphene can be modified by different heteroatom dopings. Owing to the ultrahigh electrothermal temperature (>3000 K) during the FJH process, a wide variety of dopants, such as elements (M), oxides ($MO_x$), and organic compounds ($C_xH_yM$) can be used as precursors, regardless of their boiling points or conductivities. In contrast, post-treatment methods usually depend on the vapor pressure in the gas phase or the solubility in the solution phases. Thus, the FJH synthesis allows for the direct use of various solid dopants and enables the low-cost and mass production of heteroatom-doped graphene.

密封的聚合物管防止了碳和掺杂剂的喷溅，并且可以实现高质量转化反应产率(>70%)，如图1e所示。与碳(70pm)相比，这些杂原子具有不同的原子半径(50-100pm)(图S12)。因此，在杂原子掺杂的石墨烯中存在一些晶格失配，并且在不破坏石墨结构的情况下，取代固溶体的形成被限制在一定的可行范围内。这些杂原子的电负性(2.0-4.0)不同于碳(2.5)，因此可以通过不同的杂原子掺杂来修饰石墨烯的固有电子结构。由于FJH过程中的超高电热温度(>3000 K)，各种各样的掺杂剂，例如单质(M)、氧化物($MO_x$)和有机化合物($C_xH_yM$)可以用作前体，无论其沸点或电导率如何。相反，后处理方法通常取决于气相中的蒸汽压或溶液相中的溶解度。因此，FJH合成允许直接使用各种固体掺杂剂，并且能够低成本和大规模生产掺杂杂原子的石墨烯。

Boron forms bonding types similar to that of carbon, including graphitic B ($BC_3$), borinic B ($C_2BO$), and boronic B ($CBO_2$) patterns (Figure S12). The boron-doped FG (B-FG) has good graphitic structure with B doping. The average Raman spectrum indicates 2D/G and D/G intensity ratios are 0.26 and 0.91 (Figure 3a), which indicates the good graphene

硼形成类似于碳的键合类型，包括石墨B(BC3)、硼酸B(C2BO)和硼酸B(CBO2)模式(图S12)。掺硼FG(B-FG)具有良好的石墨结构。平均拉曼光谱表明2D/G和D/G强度比分别为0.26和0.91(图3a)，这表明石墨烯质量良好，


https://doi.org/10.1021/acsnano.2c01136
ACS Nano XXXX, XXX, XXX−XXX

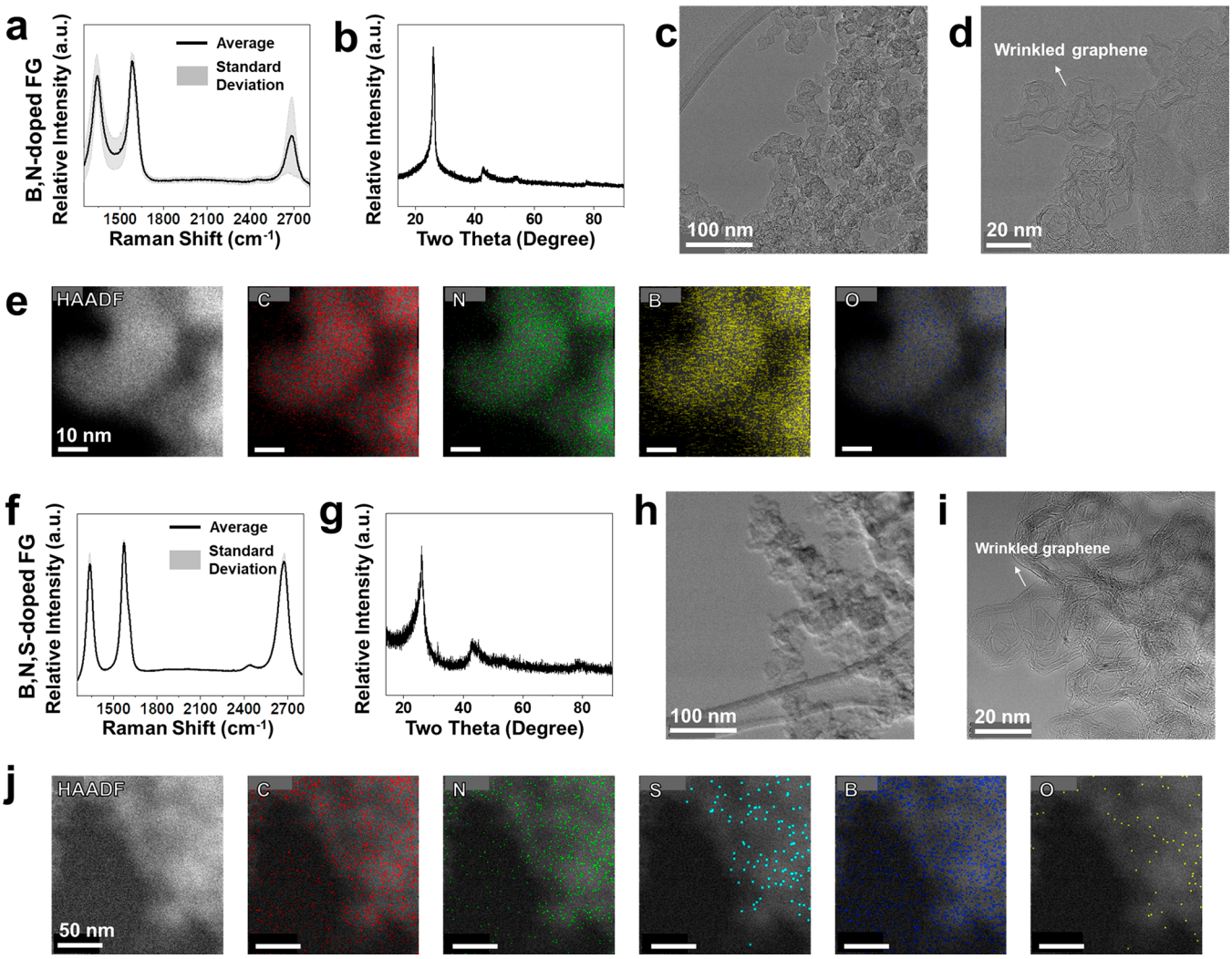


图4。闪蒸石墨烯中多个共掺杂杂原子的表征。(a)硼氮共掺杂闪蒸石墨烯的拉曼光谱。

**Figure 4. Characterization of multiple heteroatoms codoped in flash graphene. (a) Raman spectrum of B, N codoped flash graphene. The black line and the gray shadow represent the average value and the standard deviation of 100 sampling points, respectively. The same applied to the Raman spectrum below. (b) XRD result of B, N codoped flash graphene. (c) TEM and (d) HR-TEM images of B, N codoped flash graphene. (e) STEM image and corresponding elemental distribution of B, N codoped flash graphene. (f) Raman spectrum of B, N, S codoped flash graphene. (g) XRD result of B, N, S codoped flash graphene. (h) TEM and (i) HR-TEM images of B, N, S codoped flash graphene. (j) STEM image and corresponding elemental distribution of B, N, S codoped flash graphene.**

黑线和灰色阴影分别表示100个采样点的平均值和标准差。这同样适用于下面的拉曼光谱。(b)硼氮共掺杂闪蒸石墨烯的X射线衍射结果。(c)B、N共掺杂闪蒸石墨烯的TEM和(d)HR-TEM图像。(e)B、N共掺杂闪蒸石墨烯的杆像和相应的元素分布。(f)B、N、S共掺杂闪蒸石墨烯的拉曼光谱。(g)硼、氮、硫共掺杂闪蒸石墨烯的X射线衍射结果。(h)B、N、S共掺杂闪蒸石墨烯的TEM和(i)HR-TEM图像。(j)B、N、S共掺杂闪蒸石墨烯的干象和相应的元素分布。

尽管同时引入了来自B掺杂的丰富缺陷。由于导电碳反应物的平均2D/G强度比为0.06(图S13)，并且掺杂石墨烯的统计中值为0.10(表S3)，因此使用0.10的阈值来确定感兴趣的位置是否为石墨烯。

quality despite the simultaneous introduction of rich defects derived from B doping. Since the average 2D/G intensity ratio of the conductive carbon reactant is 0.06 (Figure S13), and the statistic median of doped graphene is 0.10 (Table S3), a threshold value of 0.10 is used to determine whether the site of interest is graphene. Therefore, the graphene yield of B-FG reaches 94% (Table S4). The interlayer spacing of the B-FG nanocrystals increases by 2.4% over that of commercial graphene (CG) and the average crystal size is 24.2 nm (Table S5 and Figure S14). Thermodynamic phase diagrams indicate covalent carbide $B_4C$ is the most stable state when icosahedral $B_{12}$ is used as the dopant and the local concentration of boron reaches >9%. On the other hand, the $H_3BO_3$ precursor facilitates the formation of graphitic structures without the appearance of a carbide signal in the XRD spectrum (Figure 3a). The atomic concentration of boron in B-FG is ~1.8%.

因此，B-FG的石墨烯产率达到94%(表S4)。与商用石墨烯(CG)相比，B-FG纳米晶体的层间距增加了2.4%，平均晶粒尺寸为24.2 nm(表S5和图S14)。热力学相图表明，当使用二十面体B12作为掺杂剂并且硼的局部浓度达到>9%时，共价碳化物B4C是最稳定的状态。另一方面，H3BO3前体有助于形成石墨结构，而不会在XRD光谱中出现碳化物信号(图3a)。B-FG中硼的原子浓度为1.8%。

类似地，其他气态元素(例如磷)和硫族元素(包括氧和硫)可以掺杂到FG中(图3b d，图S12)。在杂原子掺杂后石墨结构得到保留，石墨烯含量产率为86~100%，由拉曼映射确定(表S4)，而质量产率如图1e所示。

Similarly, other pnictogens such as phosphorus, and chalcogens including oxygen and sulfur, can be doped into FG (Figure 3b−d, Figure S12). After heteroatom doping, the graphitic structure is preserved, and the graphene content yields are 86−100% determined by Raman mapping (Table S4), while the mass yields are shown in Figure 1e. The heteroatom doping introduces abundant point defects and lowers the symmetry. Thus, a higher D peak ensues. Compared with intrinsic FG, with a low $I_D/I_G$ < 0.05, these doped FGs have higher $I_D/I_G$ of 0.65−0.91 (Table S4). The heteroatom-doped FGs exhibit expanded interlayer distance up to 2.7% over that of CG, and likewise have larger surface area reaching ~876 $m^2\ g^{-1}$ (Figure S15) over that of CG (~200 $m^2\ g^{-1}$) and FG (~300 $m^2\ g^{-1}$). The doped FG nanocrystals have narrow flake size distributions and have abundant micropores as well as mesopores (Figure 3b−d, Figure S15−S16). The heteroatom contents are ~1.5% for P-FG, ~5.5% for O-FG, and ~1.6% for S-FG (Figure S17), which introduce VBM of −1.91 to −2.68 eV as shown in the valence band XPS results (Figure S18).

因此，随后出现更高的D峰值。与本征FG相比，当ID/IG<0.05时，这些掺杂FG的ID/IG更高，为0.65~0.91(表S4)。异原子掺杂FG的层间距离比CG扩大了2.7%，同样比CG(200 m2/g)和FG(300 m2/g)的表面积更大，达到876 m2/g(图S15)。掺杂的FG纳米晶体具有窄的薄片尺寸分布，并且具有丰富的微孔和中孔(图3b d、图S15 S16)。杂原子含量为P-FG的1.5%、O-FG的5.5%和S-FG的1.6%(图S17)，其引入1.91至2.68 eV的VBM，如价带XPS结果所示(图S18)。

多杂原子共掺闪蒸石墨烯的表征

**Characterization of Multiple Heteroatoms Codoped in Flash Graphene.** Dual doping and multiple doping can result in synergetic effects, which may lead to a stronger

双掺杂和多掺杂可以产生协同效应，这可能比大量单杂原子对电荷密度和自旋密度的影响更大。



https://doi.org/10.1021/acsnano.2c01136
ACS Nano XXXX, XXX, XXX−XXX

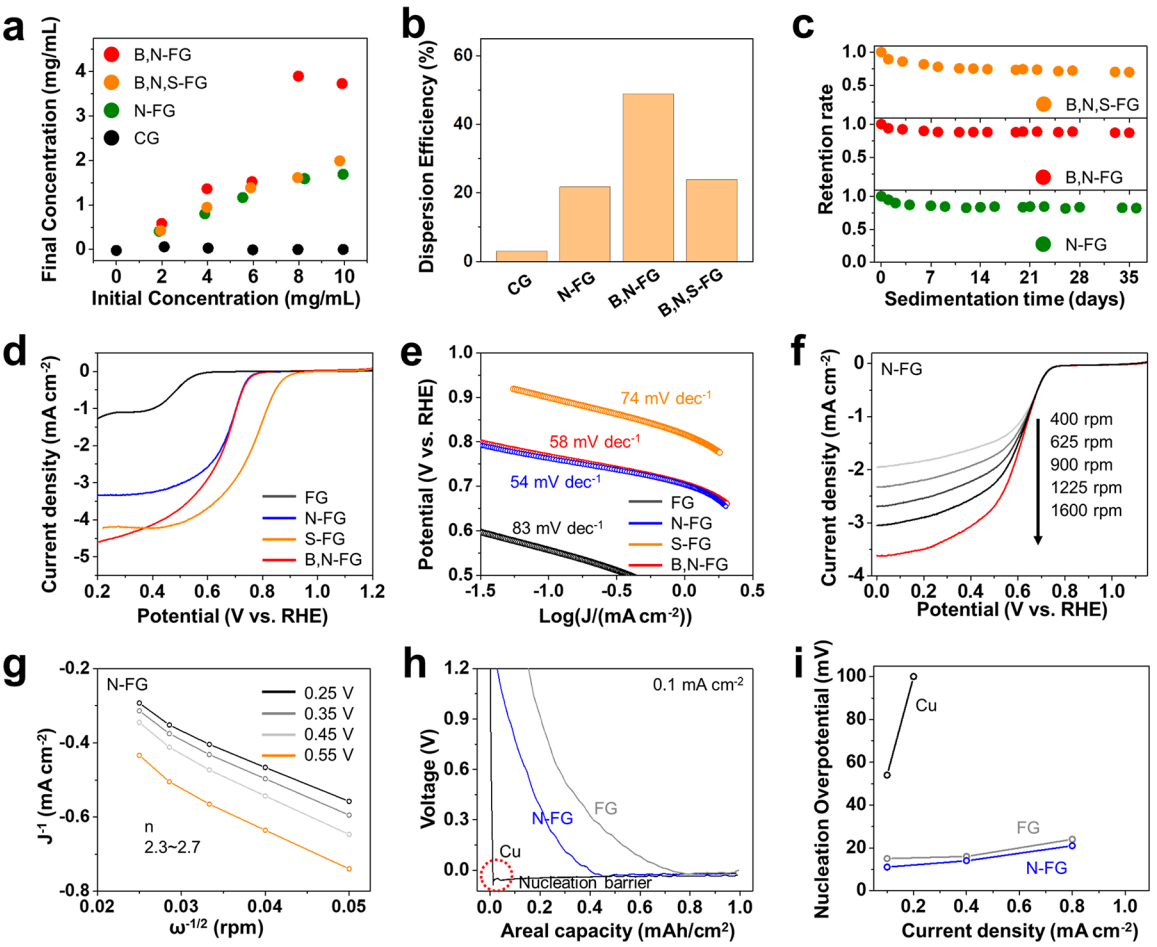


图5、杂原子掺杂闪蒸石墨烯的应用。(a)分散在水/Pluronic(F-127)(1 wt%)中的各种杂原子掺杂FG和商用石墨烯(CG)。

**Figure 5. Applications of heteroatom-doped flash graphene. (a) Various heteroatom-doped FG and commercial graphene (CG) dispersed in water/Pluronic (F-127) (1 wt %).** (b)CG和杂原子掺杂FG的分散效率。 **(b) Dispersion efficiency of CG and heteroatom-doped FG.** (c)记录沉淀时间后，不同异原子掺杂FG的保留率。 **(c) The retention rate of different heteroatom-doped FG after recorded sedimentation times.** (d)不同掺杂FG和本征FG在1600 rpm的0.1 M KOH溶液中的氧还原反应(ORR)性能和(e)相应的Tafel图。 **(d) Oxygen reduction reaction (ORR) performance of different doped FG and intrinsic FG in 0.1 M KOH solution at 1600 rpm and (e) the corresponding Tafel plots.** (f)N-FG在不同转速下的ORR极化曲线和(g)相应的K-L图。 **(f) The ORR polarization curves at different rotating rates of N-FG and (g) the corresponding K−L plots.** (h)研究了锂金属电沉积过程中铜、FG和N-FG的电压分布。 **(h) The voltage profile of Cu, FG, and N-FG during the Li metal electrodeposition.** 测试条件为0.1 mA/cm2，面积容量为1.0 mAh/cm2。 **The testing condition is 0.1 mA cm$^{-2}$ with an areal capacity of 1.0 mAh cm$^{-2}$.** (i)在不同电流密度下，锂金属电池中铜、FG和N-FG阳极的形核过电位。 **(i) The nucleation overpotential of Cu, FG, and N-FG anodes in Li metal batteries at different current densities.**

influence on charge density and spin density than a larger amount of single heteroatoms. These codoped heteroatoms with distinct chemical states can interact to provide active sites for enhancing electrocatalytic activity or introduce band structures along with local nanoscale effects. Likewise, since the entropy of mixing is higher when more distinct species are present, doping 2D materials with multiple types of heteroatoms is a viable strategy to obtain materials with high doping levels that would not be accessible with only a single dopant species. In this section, B,N-FG and B,N,S-FG are synthesized by an ultrafast and all-solid-state catalyst-free FJH method. As-synthesized B,N-FG has a good graphene structure (Figure 4a), and the graphene content yield reaches 89% (Table S4). Dual doping causes abundant point defects and a high average $I_D/I_G$ ~ 0.90 is obtained from 100 sampling points. The interlayer spacing of B,N-FG increases 2.6% (Figure 4b) compared to CG and the average particle size is 49.9 nm (Table S5, Figure S19). B,N-FG has a large surface area of 393 m$^2$ g$^{-1}$ and abundant micropores and mesopores (Figure S20). HR-TEM images show the presence of lattice fringes and wrinkled structures of doped FG nanoparticles (Figure 4c,d). The uniform distribution of B, C, and N in these nanoparticles is shown in Figure 4e. High resolution XPS spectra indicate that the total amount of B and N is 10.4% (Figure S21), which is higher than the fraction achieved when using only N or B dopant atoms alone. Emerging bonding states between heteroatoms, B and N, can be found in B 1s and N 1s spectra (Figure S21), and B,N-FG has a large VBM −3.02 eV (Figure S22). Similar results are found in B,N,S-FG. The graphene content yield and $I_D/I_G$ are 87% and 0.83, respectively (Figure 4f, Table S4). The interlayer spacing of B,N,S-FG is 2.2% larger than CG (Figure 4g) and the average particle size is 76.0 nm (Figure 4h, Figure S19). These nanocrystals exhibit similar wrinkled structures and homogeneous elemental distribution of B, N, and S (Figure 4i,j). The total atomic content for these three types of heteroatoms is ~13.5% and additional bonding states between heteroatoms, B and N, can be observed (Figure S23). The VBM of B,N,S-FG is −2.54 eV (Figure S22).

这些具有不同化学状态的共掺杂杂原子可以相互作用以提供活性位点以增强电催化活性或引入带结构以及局部纳米级效应。同样，由于混合熵在存在更多不同物种时更高，因此用多种类型的杂原子掺杂2D材料是一种可行的策略，以获得仅用单一掺杂剂物种无法获得的高掺杂水平的材料。在本节中，B、N-FG和B、N、S-FG是通过超快全固态无催化剂FJH方法合成的。合成B时，N-FG具有良好的石墨烯结构(图4a)，石墨烯含量产率达到89%(表S4)。双掺杂导致大量的点缺陷，从100个采样点获得高平均ID/IG~0.90。与CG相比，B,N-FG的层间距增加了2.6%(图4b)，平均粒径为49.9 nm(图S19)。B,N-FG具有393 m2/g的大比表面积和丰富的微孔和中孔(图S20)。HR-TEM图像显示掺杂FG纳米颗粒的晶格条纹和褶皱结构的存在(图4c，d)。B、C和N在这些纳米颗粒中的均匀分布如图4e所示。高分辨率XPS光谱表明，B和N的总量为10.4%(图S21)，高于仅使用N或B掺杂原子时获得的分数。在B 1s和N 1s光谱中可以发现杂原子B和N之间出现的键合状态(图S21)，并且B，N-FG具有较大的VBM 3.02 eV(图S22)。在B、N、S-FG中也发现了类似的结果。石墨烯含量产率和ID/IG分别为87%和0.83(图4f，表S4)。B,N,S-FG的层间距比CG大2.2%(图4g)，平均粒径为76.0 nm(图4h，图S19)。这些纳米晶体表现出类似的褶皱结构和B、N和S的均匀元素分布(图4i，j)。这三种杂原子的总原子含量为13.5%，可以观察到杂原子B和N之间的附加键状态(图S23)。B,N,S-FG的VBM为2.54 eV(图S22)。

### Scaling up and Applications of Heteroatom-Doped Flash Graphene.

杂原子掺杂闪蒸石墨烯的放大及应用

Gram-scale N-FG (N-FG-L2) synthesis is demonstrated in this section, and the graphene quality along with properties of N-FG-L2 are similar to those of N-FG synthesized from the small batch. The graphene content yield and $I_D/I_G$ of N-FG-L2 are 99% and 1.08, respectively (Table S4, Figure S24), which reflects the abundance of point defects

本节演示了克级N-FG(N-FG-L2)合成，N-FG-L2的石墨烯质量和性能与小批量合成的N-FG相似。N-FG-L2的石墨烯含量产率和ID/IG分别为99%和1.08(表S4，图S24)，这反映了点缺陷和六角形对称的局部破缺的丰富性。


https://doi.org/10.1021/acsnano.2c01136
ACS Nano XXXX, XXX, XXX−XXX

在26.0度处有一个

and local breaking of hexagonal symmetry. There is an

不对称的(002)衍射峰，表明层间距离扩大了2.1%。

asymmetrical (002) diffraction peak at ~26.0 degree, which

indicates the expansion of interlayer distance by ~2.1%. The

N-FG-L2的平均尺寸为41.2 nm(图S25)，表面积为573 m2/g。N-FG-L2的孔径分

average size of N-FG-L2 is 41.2 nm (Figure S25) and the

布与N-FG相似。

surface area is 573 $m^2\ g^{-1}$. Pore size distribution of N-FG-L2 is

高分辨率的N 1s光谱表明，N的原子比为3.1%，吡啶氮和吡咯氮占

similar to N-FG. The high-resolution N 1s spectrum shows the

主导地位，它们与金属和其他正电荷物种有很强的结合能。

atomic ratio of N is ~3.1%, and pyridinic N and pyrrolic N are

dominant, which have strong binding energies with metals and

other electropositive species.[10]

杂原子掺杂的FG可分散在水-Pluronic(F-127)表面活性剂(1 wt%)溶液中，与

Heteroatom-doped FG is dispersible in water-Pluronic (F-

本征FG类似，它们提供高浓度的分散，达到4mg

127) surfactant (1 wt %) solution and similar to intrinsic FG,

they give highly concentrated dispersions reaching ~4 mg

(图5a，图S26)。 该结果与CG不同，CG在1 wt%F-127水溶

$mL^{-1}$ (Figure 5a, Figure S26). This result is distinct from

液中的分散性很小(图5b，图S27)。

CG, which shows little dispersibility in 1 wt % F-127 aqueous

分散效率衡量石墨烯的最终分散浓度

solution (Figure 5b, Figure S27). The dispersion efficiency

和初始浓度之间的比率。

measures the ratio between final dispersed concentration and

N-FG、B、N-FG和B、N、S-FG的色散效率分

initial concentration of graphene. The dispersion efficiencies of

别是CG的8、17和8倍，这可以归因于杂原子掺杂FG的涡轮层排列允许有效剥离。

N-FG, B,N-FG and B,N,S-FG are ~8, ~17, and ~8 times

higher than that of CG, respectively, which can be attributed to

the turbostratic arrangement of heteroatom-doped FG

allowing efficient exfoliation. 剥离所需的分散力远低于通过石墨剥离获得的 The dispersion force needed

传统AB堆叠石墨烯中的分散力。

for exfoliation is much lower than that need in conventional

AB-stacked graphene obtained by graphite exfoliation. The

分散液具有很高的时间稳定性，35天后，N-FG、B、N-FG和B、N、S-FG的保留率分别为82%、86%

dispersions show high temporal stability, and after 35 days, the

和69%(图5c)。

retention rates of N-FG, B,N-FG and B,N,S-FG are 82%, 86%,

在其他有机溶剂中，例如N，N-二甲基

and 69%, respectively (Figure 5c). In other organic solvents,

甲酰胺(DMF)和N-甲基-2-吡咯烷酮(NMP)，N-FG也表现出良好的分散性。N-FG在

such as *N,N*-dimethylformamide (DMF) and *N*-methyl-2-

DMF中的分散效率比CG高40.4倍和8.2倍(图S28)。

pyrrolidone (NMP), N-FG also shows great dispersibility and

the dispersion efficiencies of N-FG in DMF, and NMP solvents

are ~40.4 and ~8.2 times higher than that of CG (Figure

S28).[39]

为了证明杂原子掺杂FG作为电催化剂的适用性，测试了各种掺杂FG的电化学ORR性能。

To demonstrate the applicability of heteroatom-doped FG

as electrocatalysts, the electrochemical ORR performances of

五种不同掺杂FG和本征FG的极化曲线如图5d和

various doped FG are tested. The polarization curves of five

图S29所示。在无金属电催化剂中，S-FG显示出最优越的ORR活性。

different doped FG and intrinsic FG are shown in Figure 5d

and Figure S29. S-FG shows the most superior ORR activity

0.2 mA/cm2下的电势为0.88V，

among the metal-free electrocatalysts. The potential at 0.2 mA

塔菲尔斜率为74 mV/dec(图5e，表S6)。

$cm^{-2}$ is 0.88 V and the Tafel slope is 74 mV $dec^{-1}$ (Figure 5e,

S-FG在1600 rpm时的饱和电流密度达到4.2 mA/cm2。

Table S6). The saturated current density of S-FG at 1600 rpm

电子转移数(n)对于确定ORR的最终产物很重要，

reaches ~4.2 mA $cm^{-2}$. The electron transfer number ($n$) is

可以通过库特基-列维奇方程(K-L方程)进行估计。

important to determine the final product of ORR and it can be

estimated by the Koutecký−Levich equation (K-L equation).[40]

不同转速下N-FG的极化曲线和相应的K-L图如图5f和g所示。

The polarization curves of N-FG at different rotating rates and

the corresponding K-L plots are shown in Figure 5f and g. And

对于N-FG，n为2.3-2.7，这表明H2O2可能是主要产物。

$n$ is 2.3−2.7 for N-FG, which indicates $H_2O_2$ can be the major

杂原子共掺导致不同的化学状态和协同效应。

product. Heteroatom codoping results in distinct chemical

对于B,N-FG，n接近4，这表明H2O是主要产物

states and synergistic effects. For B,N-FG, $n$ is close to 4, which

(图S30)。 N-FG和B,N-FG的

suggests $H_2O$ is the major product (Figure S30). The stability

稳定性测试表明，在1000次循环后，过电位增加，电流密度降低，这表明性能下降，可能

tests of N-FG and B,N-FG show the increase of overpotentials

与亚稳结构有关(图S30)。

and the decrease of current densities after 1000 cycles, which

indicates the degradation of performance and might relate to

由于之前的研究表明，微量金属

the metastable structures (Figure S30). Since previous studies

也有助于碳材料的电化学性能，我们进行了ICP-MS，以分析反应物和产物中14种

have shown that trace metals can also contribute to the

不同微量金属的含量：Cr、Co、Fe、Mn、Ni、V、W、Pt、Mo、Ir、Pd、Au、Ti和Ru(图

electrochemical performance of the carbon materials, we

S31 34)。

carried out ICP-MS to analyze the content of 14 different trace

metals: Cr, Co, Fe, Mn, Ni, V, W, Pt, Mo, Ir, Pd, Au, Ti, and

Ru, in the reactants and the products (Figures S31−34). The

结果表明，不同样品中这些金属的含量远低于先前文献中报告的值。

results show that the content of these metals from different

samples are much lower than the values reported in the

因此，反应物和闪蒸反应对产物的污染最小，对ORR的影响很小。

previous literature. Therefore, the reactants and flash

reaction will cause minimal contamination of the products and

little effect on the ORR.

由于N中存在孤对电子，其与金属原子(如Li)提供强大的结合能，因此N-FG被用作

Since there are lone pair electrons in N, which provides

锂金属电池的电极材料。

strong binding energies with metal atoms such as Li, N-FG is

used as an electrode material in a lithium metal battery.[10]

与裸铜电极(54 mV)相比，N-FG在0.1 mA/cm2下的金属锂电沉积过程中表现出较小

Compared to bare Cu electrode (54 mV), N-FG exhibits a

的形核过电位(11 mV)(图5h)，这表明N-FG的形核势垒较小。

smaller nucleation overpotential (11 mV) during the electro-

deposition of metallic Li at 0.1 mA $cm^{-2}$ (Figure 5h), which

indicates a smaller nucleation energy barrier for N-FG. A

较小的成核势垒有助于形成更均匀的原子核和随后均匀的金属锂沉积。

smaller energy barrier for nucleation facilitates the formation of

more homogeneous nuclei and subsequent uniform metallic Li

N-FG的成核过电位小于FG(图5i)，因为N-FG的结合能比内在FG

deposition.[14,15] The nucleation overpotential for N-FG is

更强。

smaller than that of FG (Figure 5i), because the binding energy

这一结果与之前的文

of N-FG is stronger than in intrinsic FG. This result is

献报告一致。

consistent with a previous literature report.[10]

## CONCLUSION

总之，七种不同的杂原子掺杂FG，包括单元素掺杂的N-FG、B-FG、O-FG、P-FG、S-FG、双

In conclusion, seven different heteroatom-doped FG, including

元素共掺杂的B,N-FG和多元素共掺杂的B,N,S-FG，通过超快全固态无催化剂、无溶剂和无水

single element doped N-FG, B-FG, O-FG, P-FG, S-FG, dual

FJH方法直接合成。

elements codoped B,N-FG, and multiple elements codoped

B,N,S-FG, are directly synthesized by an ultrafast and all-solid-

无论沸点和

state catalyst-, solvent-, and water-free FJH method. Different

电导率如何，都可以使用不同的低成本掺杂剂，包括单质、氧化物和有机化合物。

low-cost dopants, including elements, oxides, and organic

compounds can be used regardless of boiling point and

合成的掺杂FG具有良好的石墨烯质量、涡轮层状结构和扩展的层间距。

conductivity. The as-synthesized doped FG has good graphene

quality, turbostratic structure, and expanded interlayer spacing.

因此，它们可分散在水Pluronic(F-127)(1 wt%)溶液中，然后形成稳定的浓缩分

Therefore, they are dispersible in water-Pluronic (F-127) (1 wt

散液。

%) solution, and then form stable concentrated dispersions.

杂原子掺杂改变了电子结构，提高了掺杂FG作为电催化剂和电化学储能材料的性能。

Heteroatom doping modifies the electronic structures, which

improves the performance of doped FG as electrocatalysts and

掺杂FG的克级合成也证

electrochemical energy storage materials. The gram-scale

明了FJH方法对生产的可扩展性。

synthesis of doped FG is also demonstrated to show the

杂原子掺杂FG合成

scalability of the FJH method to bulk quantities. The electrical

的电能成本仅为1.2-10.7 kJ/g，

energy cost for heteroatom-doped FG synthesis is only 1.2−

这可以使FJH方法适用于低成本和大规模生产掺杂杂原子的石墨烯。

10.7 kJ $g^{-1}$, which could render the FJH method suitable for

low-cost and mass production of heteroatom-doped graphene.

由于目前使用类似的FJH技术将内在FG的产量扩大到每天1吨，因此，此处的技术应易于

Since the intrinsic FG is currently being scaled to 1-ton per day

转换为类似规模。

production using an analogous FJH technology,[46] the protocol

here should be easily translated to similar scales.

实验部分

## EXPERIMENTAL SECTION

材料。 炭黑(CB，APS 10 nm，黑珍珠2000)购自卡博特公司。

**Materials.** Carbon black (CB, APS 10 nm, Black Pearls 2000) was

三聚氰胺(M2659-1KG，99%)购自密理博西

purchased from Cabot Corporation. Melamine (M2659-1KG, 99%)

硼酸(31768-453.6G，

was purchased from Millipore-Sigma. Boric acid (31768-453.6G,

99.9%)购自贝克分析试剂。 蔗糖(

99.9%) was purchased from Baker Analyzed Reagent. Sucrose

SX1075-1500g，ACS级)购自MilliporeSigma。

(SX1075-1, 500G, ACS grade) was purchased from Millipore-

红磷(343242-5G，99.99%)购自密理博西格玛。

Sigma. Red phosphorus (343242-5G, 99.99%) was purchased from

聚(1,4-苯硫醚)(PPS，182354-100G，平均锰10000)购自密理博西

Millipore-Sigma. Poly(1,4-phenylene sulfide) (PPS, 182354-100G,

硼粉(

average Mn ~ 10 000) was purchased from Millipore-Sigma. Boron

11337-10G，无定形，325目)购自Alfa Aesar。

powder (11337-10G, amorphous, ~325 mesh) was purchased from

使用石墨垫片和碳化钨圆柱杆(直径4 mm)作为电极。

Alfa Aesar. Graphite spacers and tungsten carbide cylinder rods (4

FJH反应容器采用聚四氟乙烯管、

mm diameter) were used as the electrodes. Polytetrafluoroethylene

聚苯硫醚管或聚丙烯腈管(内径=4mm，外径=25mm，长度=6cm)。

tubes, poly(1,4-phenylene sulfide) tubes or polyacrylonitrile tubes (ID

= 4 mm, OD = 25 mm, length = 6 cm) were used as the FJH reaction

xGnP石墨纳米片(xGnP-15，序列号#：5051209)从XG Sciences获得，并用作比较。

vessels. xGnP graphite nanoplatelets (xGnP-15, serial #: 5051209)

were obtained from XG Sciences and were used as received for the

商业石墨烯来自天元帝国。

comparison. Commercial graphene was obtained from Tianyuan

Empire。

对于分散测试，Pluronic(F-127，P2443-250G)从Millipore Sigma购买。

For the dispersion tests, the Pluronic (F-127, P2443-250G) was

对于电化学测试，氢氧化钾(KOH，

purchased from Millipore-Sigma. For the electrochemical tests,

221473-500G，ACS级)从密理博西格玛公司购买。

potassium hydroxide (KOH, 221473-500G, ACS grade) was

对于电池测试，N-甲基吡咯烷酮(NMP，>99.0%

purchased from Millipore-Sigma. For the battery tests, *N*-methyl

，443778-500ML)从密理博西格玛公司购买。

pyrrolidone (NMP, >99.0%, 443778-500ML) was purchased from

球磨(钇稳定氧化锆，99.5%，R=5±0.3 mm)从MTI公司购买。

Millipore-Sigma. The milling ball (Yttrium stabilized $ZrO_2$, 99.5%, R

双(三氟

= 5 ± 0.3 mm) was purchased from MTI Corporation. Lithium

甲烷磺酰基)亚胺锂(LiTFSI，99.95%，痕量金属基，544094-25G)购自密理博西格玛。

bis(trifluoromethanesulfonyl)imide (LiTFSI, 99.95%, trace metals

basis, 544094-25G) was purchased from Millipore-Sigma. Lithium



https://doi.org/10.1021/acsnano.2c01136
ACS Nano XXXX, XXX, XXX−XXX

硝酸锂(LiNO3，99.99%，微量金属基，229741-25G)购自密理博西格玛。
nitrate ($LiNO_3$, 99.99%, trace metals basis, 229741-25G) was
1,2-二甲氧基乙烷(二甲醚，无水，99.5%
purchased from Millipore-Sigma. 1,2-dimethoxyethane (DME,
无抑制剂，259527-100ML)购自密理博西格玛。
anhydrous, 99.5% inhibitor-free, 259527-100ML) was purchased
1,3-二氧戊环(DOL，无水，99.8%，75 ppm BHT作为抑制剂，
from Millipore-Sigma. 1,3-Dioxolane (DOL, anhydrous, 99.8%, ~75
271020-1L)购自MilliporeSigma。
ppm BHT as inhibitor, 271020-1L) was purchased from Millipore-
聚偏氟乙烯粘合剂(PVDF，121120-80G)购自MTI公司。
Sigma. Poly(vinylidene fluoride) binder (PVDF, 121120-80G) was
高导电乙炔炭黑(ABHC-01342431)购自
purchased from MTI Corporation. High conductive acetylene black
Soltex Corporation。
(ABHC-01 342431) was purchased from Soltex Corporation.
对于电感耦合等离子体质谱(ICP-MS)测试，HNO3(67 70 wt%，痕量金属级，费希尔化学)、
For the inductively coupled plasma mass spectrometry (ICP-MS)
HCl(37 wt%，99.99%痕量金属基，微孔西格玛)、水(微孔西格玛，ACS超痕量分析试剂)
tests, $HNO_3$ (67−70 wt %, TraceMetal grade, Fisher Chemical), HCl
和所有标准品(周期表混合物)均从微孔西格玛购买。
(37 wt %, 99.99% trace metals basis, Millipore-Sigma), water
(Millipore-Sigma, ACS reagent for ultratrace analysis), and all the
standards (periodic table mixtures) were purchased from Millipore-
Sigma.

表征 使用FEI Helios NanoLab 660双光束扫描电镜，在5 kV电压
**Characterization.** The reactant and flash products were
下，工作距离为4 mm，通过扫描电子显微镜(SEM)对反应物和闪蒸产物进行了表征。
characterized through scanning electron microscopy (SEM) using a
FEI Helios NanoLab 660 DualBeam SEM at 5 kV with a working
使用JEOL 2100F场发射枪透射电子显微镜在200 kV下拍摄TEM图像。
distance of 4 mm. TEM images were taken with a JEOL 2100F field
在精确的球差
emission gun transmission electron microscope at 200 kV. HR-TEM
校正后，使用FEI Titan Themis S/TEM仪器在300 keV下拍摄HR-TEM和HAADF-STEM图像。
and HAADF-STEM images were taken with FEI Titan Themis S/
TEM instrument at 300 keV after accurate spherical aberration
使用PHI-Quantera SXM扫描X射线微探针在5×10 9托的基压下收集X射线光电子
correction. X-ray photoelectron spectroscopy (XPS) data were
能谱(XPS)数据。
collected with a PHI Quantera SXM Scanning X-ray Microprobe
使用0.5 eV步长记录测量光谱，通过能量
with a base pressure of $5 \times 10^{-9}$ Torr. Survey spectra were recorded
为140 eV。
using 0.5 eV step sizes with a pass energy of 140 eV. Elemental spectra
使用0.1 eV步长记录元
素光谱，通过能量为26 eV。
were recorded using 0.1 eV step sizes with a pass energy of 26 eV. All
使用C 1s峰(284.8 eV)作为参考对所有XPS光谱进行校正。
of the XPS spectra were corrected using the C 1s peaks (284.8 eV) as
X射线衍射(XRD)测量由Rigaku SmartLab智能XRD系统进行，过滤铜钾辐射
reference. X-ray diffraction (XRD) measurements were done by a
(λ=1.5406)。
Rigaku SmartLab Intelligent XRD system with filtered Cu Kα
使用功率为5 mW的532 nm激光，使用Renishaw拉曼显微
radiation ($\lambda$ = 1.5406 Å). Raman spectra were collected with a
镜收集拉曼光谱。
Renishaw Raman microscope using a 532 nm laser with a power of 5
使用50×透镜进行局部拉曼光谱和拉曼映射。
mW. A 50× lens was used for local Raman spectra and Raman
使用UV-vis(岛津UV-3600 plus)收集反应物和闪蒸产物悬浮液的光谱。
mapping. UV−vis (Shimadzu UV-3600 plus) was used to collect the
使用Thermo
spectra of the suspension of reactant and flash products. A Thermo
Scientific Nicolet 6700衰减全反射傅立叶变换红外光谱仪(ATR-FTIR)分析反应物和闪蒸产
Scientific Nicolet 6700 attenuated total reflectance Fourier-transform
物中的振动和旋转模式。
infrared (ATR-FTIR) spectrometer (Waltham, MA) was used to
analyze the vibration and rotation modes in the reactant and the flash
product.

FJH系统。 电路图和FJH反应箱如图S1所示。
**FJH System.** The circuit diagram and FJH reaction box were
在机器车间制备厚壁聚合物管(ID=4 mm，OD=25 mm，长度=6 cm)，
shown in Figure S1. A thick-walled polymer tube (ID = 4 mm, OD =
并用于装载反应物粉末。
25 mm, length = 6 cm) was prepared in a machine shop and used to
使用石墨垫片(D=4 mm，长度=5 mm)和碳化钨圆柱杆
load the reactant powder. Graphite spacers ($D$ = 4 mm, length = 5
(D=4 mm，长度=5 cm)作为电极来压缩加载的粉末。
mm) and tungsten carbide cylinder rods ($D$ = 4 mm, length = 5 cm)
were utilized as electrodes to compress the loaded powder. The
石墨垫片与样品接触，碳化钨圆柱杆与电路连接。
graphite spacers were in contact with the samples and tungsten
在这项工作中，使
carbide cylinder rods were connected with the circuit. In this work,
用不同的前驱体来制备掺杂杂原子的FG。
different precursors were used to prepare heteroatom doped FG. The
反应物包括(1)炭黑、(2)三聚氰胺和炭黑、(3)硼酸和炭黑、(4)蔗糖和炭黑、(5)
reactants included a mixture of (1) CB, (2) melamine and CB, (3)
红磷和炭黑、(6)聚苯硫醚和炭黑、(7)硼、三聚氰胺和炭黑的混合物，以及(8)硼、三
boric acid and CB, (4) sucrose and CB, (5) red phosphorus and CB,
聚氰胺、聚苯硫醚和炭黑的混合物。
(6) PPS and CB, (7) boron, melamine, and CB, and (8) boron,
电能由总电容为60 mF的电路中的电容器组提供。
melamine, PPS, and CB. The electrical energy was provided by a
capacitor bank in the circuit with a total capacitance of 60 mF. The
电容器组由可达到400 V的电源直流充电。
capacitor bank was charged by a d.c. supply that could reach 400 V.
闪蒸持续时间由电路中充当高速开关的Arduino控制器继电器控制。
The flash duration was controlled by an Arduino controller relay in
不同反应物的反应物电阻不同，改变闪
the circuit acting as a high-speed switch. The reactant resistances for
蒸条件以控制总输入电热能。
various reactants were different, and the flash conditions were
为了扩大N-FG，
changed to control the total input electrothermal energy. To scale up
N-FG-L1使用了厚壁聚合物管(ID=8 mm，OD=25 mm，长度=6 cm)和石墨垫片(D=8 mm，长度
the N-FG, thick-walled polymer tube (ID = 8 mm, OD = 25 mm,
=5 mm)。
length = 6 cm) and graphite spacers ($D$ = 8 mm, length = 5 mm) were
石英管(内径=16 mm，外径=20 mm，长度=6 cm)和石墨垫片
used for N-FG-L1. The quartz tube (ID = 16 mm, OD = 20 mm,
(直径=16 mm，长度=3 cm)用于N-FG-L2。
length = 6 cm) and graphite spacers ($D$ = 16 mm, length = 3 cm)
根据表S1中的能量密度计算输入电热能。
were used for N-FG-L2. And the input electrothermal energy was
参数如表1所示。
calculated based on the energy densities in Table S1. The parameters
表1优化了各种样品的重量比。
are listed in Table 1. The weight ratios of various samples are
我们试图优化最终条件的四个因素：
optimized in Table 1. There are four factors for which we try to
optimize the final conditions:

均匀闪蒸反应。 我们将均匀混合的反应物的电阻控制在0.4到
1. Homogeneous flash reactions. We control the resistance of the
5.0之间，并监控
evenly mixed reactants between 0.4−5.0 Ω, and monitor the
确保均匀闪蒸反应的电流-时间(I-t)曲线
current−time ($I$−$t$) curves to ensure a homogeneous flash
reaction
涡轮层状石墨烯的形成。 拉曼光谱和X射线衍射用于检查
2. The formation of turbostratic graphene. Raman and XRD are
涡轮层石墨烯的形成，以筛选条件。
used to check the formation of turbostratic graphene to screen
the condition.
sp2-C和杂原子之间键的形成。
3. The formation of bonds between $sp^2$-C and heteroatom. Since
由于目的是制备掺杂石墨烯，因此应排除sp3-C和杂原子之间键合的可能性。
the purpose is to prepare doped graphene, the possibility of
XPS用
bonds between $sp^3$-C and heteroatom should be excluded. XPS
于分析键合状态。
is used to analyze the bonding states.
杂原子的含量。 XPS用于分析杂原子的含量。
4. The contents of the heteroatom. XPS is used to analyze the
contents of the heteroatom.

有关FJH设置的更多安全说明和电路图，请参阅支持信息和我们以前的出版物。
More safety notes and a circuit diagram of the FJH setup are in the
注意！
Supporting Information and our previous publications. ***Caution!***
确保遵守所有安全预防措施以减轻触电。
*Ensure that all safety precautions are observed to mitigate electrocution. As*
最后一项措施是，一定要戴到肘部的厚橡胶手套。
*a last measure, be sure to wear thick rubber gloves that extend to the*
FJH反应后，建议让装置冷却并通风3-5分钟。
*elbows. After the FJH reaction, it is suggested to allow the apparatus to*
并确保电容器组已通过断路器(而不是拨动开关)与系统分
*cool and vent for 3−5 min. And ensure that the capacitor bank has been*
离，并且电容器组已完全放电。
*separated from the system by a circuit breaker (not a toggle switch), and*
*that the capacitor bank has been fully discharged.*

电化学测试。 氧还原反应(ORR)。
**Electrochemical Tests.** Oxygen reduction reaction (ORR). The
通过将2 mg杂原子掺杂FG分散在2 mL粘合剂溶液中制备浆料，该粘合剂溶液为160 L 5 wt%Nafion溶
slurry was prepared by dispersing 2 mg heteroatom doped FG in 2 mL
液，混合在2 mL水/乙醇(1:1，体积比)中。
binder solution, which is 160 $\mu$L of 5 wt % Nafion solution mixed in 2
将浆料超声处理30分钟以形成均匀的油墨。
mL water/ethanol (1:1, volume ratio). The slurry was sonicated for
将体积为20 L的油墨溶液加载到玻璃碳
30 min to form a homogeneous ink. A volume of 20 $\mu$L of ink
电极(直径为5 mm)上，并在室温下在空气中干燥。
solution was loaded onto a glassy carbon electrode (5 mm in
使用CHI 608D电化学工作站
diameter) and dried in air at room temperature. The electrochemical
在三电极配置中进行电化学测量。
measurements were carried out in a three-electrode configuration
石墨棒和HgO/Hg(1 M
using a CHI 608D electrochemical workstation. A graphite rod and
KOH)电极分别用作计数器和参比电极。
HgO/Hg (1 M KOH) electrode were used as the counter and
电解液为0.1 M KOH，注入氧气以达到氧气饱和。
reference electrodes, respectively. The electrolyte was 0.1 M KOH
以100 mV s1的扫描速率，在1.2至
sparged with $O_2$ gas for $O_2$ saturation. CV was carried out with
0 V(vs RHE)的电位范围内进行10个周期的CV。LSV的电位范围为1.2到
potential ranging from 1.2 to 0 V (vs RHE) for 10 cycles at a scan rate
of 100 mV $s^{-1}$. LSV was carried out with potential ranging from 1.2 to
0 V(vs RHE)，扫描速率为5 mV/s。
0 V (vs RHE) at a scan rate of 5 mV $s^{-1}$.
在电池测试中，通过以0.9:0.1的比例研磨掺杂FG和聚三氟乙烯(PVDF)的混合物来制备电极。
For the battery tests, the electrode was prepared by grinding the
mixture of doped FG, and poly(vinyl difluoride) (PVDF) at a ratio of
使用少量(总质量的3倍)N-甲基吡咯烷酮形成均匀浆料。
0.9:0.1. A small amount (~3× of the total mass) of $N$-methyl
pyrrolidone was used to form a homogeneous slurry. The slurries
通过在1500 rpm
下球磨10分钟形成浆液。
were formed by ball milling at 1500 rpm for 10 min. The current
集电器为厚度为
10 μm的铜箔。 用刮墨刀将浆料施加到
collector was Cu foil with a thickness of 10 $\mu$m. The slurry was
铜箔上，刮墨刀间距为100 μm。
applied to the Cu foil by a doctor blade with a blade spacing of 100
使用放置在电极顶部的内置加热盖在70 °C下干燥电极2小时，然后将其放入真空炉中过夜。
$\mu$m. The electrode was dried using a built-in heating cover placed on
top of the electrode at 70 °C for 2 h and was then put in a vacuum
真空烘箱的温度和压力设置为70 °C和10 mmHg。
oven overnight. The temperature and pressure of the vacuum oven
阴极面积为2.0 cm2。
were set at 70 °C and ~10 mmHg. The area of the cathode was ~2.0
使用的电解液为1 M LiTFSI，在二甲醚和DOL(V:V=1:1)的混合物中，添加2%的LiNO3作
$cm^2$. The electrolyte used was 1 M LiTFSI in a mixture of DME and
为添加剂。 每个币形电池中的电解液
DOL (V:V = 1:1) with 2% $LiNO_3$ as the additive. The volume of the
体积为30 μL。
electrolyte in each coin cell was 30 $\mu$L.

## ASSOCIATED CONTENT

### Supporting Information

The Supporting Information is available free of charge at https://pubs.acs.org/doi/10.1021/acsnano.2c01136.

Safety instructions, TEM, SEM, and other images; XPS and Raman spectra; Additional graphs (PDF)

## AUTHOR INFORMATION

### Corresponding Author

**James M. Tour** − *Department of Chemistry, Department of Materials Science and NanoEngineering, Smalley-Curl Institute, the NanoCarbon Center, and The Welch Institute for Advanced Materials, and Department of Computer Science, Rice University, Houston, Texas 77005, United States;* orcid.org/0000-0002-8479-9328; Email: tour@rice.edu


https://doi.org/10.1021/acsnano.2c01136
ACS Nano XXXX, XXX, XXX−XXX

### Authors

**Weiyin Chen** — *Department of Chemistry, Rice University, Houston, Texas 77005, United States*

**Chang Ge** — *Department of Chemistry and Applied Physics Program, Rice University, Houston, Texas 77005, United States*

**John Tianci Li** — *Department of Chemistry and Department of Materials Science and NanoEngineering, Rice University, Houston, Texas 77005, United States;* orcid.org/0000-0002-7218-8298

**Jacob L. Beckham** — *Department of Chemistry, Rice University, Houston, Texas 77005, United States*

**Zhe Yuan** — *Department of Chemistry, Rice University, Houston, Texas 77005, United States*

**Kevin M. Wyss** — *Department of Chemistry, Rice University, Houston, Texas 77005, United States*

**Paul A. Advincula** — *Department of Chemistry, Rice University, Houston, Texas 77005, United States*

**Lucas Eddy** — *Department of Chemistry and Applied Physics Program, Rice University, Houston, Texas 77005, United States*

**Carter Kittrell** — *Department of Chemistry, Rice University, Houston, Texas 77005, United States;* orcid.org/0000-0002-8449-4292

**Jinhang Chen** — *Department of Chemistry, Rice University, Houston, Texas 77005, United States*

**Duy Xuan Luong** — *Department of Chemistry, Rice University, Houston, Texas 77005, United States;* orcid.org/0000-0001-7089-3359

**Robert A. Carter** — *Department of Chemistry, Rice University, Houston, Texas 77005, United States*

Complete contact information is available at: https://pubs.acs.org/10.1021/acsnano.2c01136


### Author Contributions

[#]W.C. and C.G. contributed equally to this work.

### Notes

The authors declare the following competing financial interest(s): Rice University owns intellectual property on flash graphene. Some of that intellectual property has been licensed to Universal Matter Inc. J.M.T. is a stockholder in Universal Matter, but he is not an officer, director, or employee. Conflicts of interest are mitigated through regular disclosures to and compliance with the Rice University Office of Sponsored Programs and Research Compliance. D.X.L. was employed by Rice University when this work was done. He is now employed by Universal Matter.

## ACKNOWLEDGMENTS

The funding of the research is provided by Air Force Office of Scientific Research (FA9550-19-1-0296), DOE-NETL (DE-FE0031794), and U.S. Army Corps of Engineers, ERDC (W912HZ-21-2-0050). The characterization equipment used in this project is from the Shared Equipment Authority (SEA) at Rice University. The authors acknowledge the use of the Electron Microscopy Center (EMC) at Rice University. We thank Dr. Bo Chen for helpful discussion of the XPS results, and Dr. Chris Pennington for method development of the ICP-MS tests. We thank Prof. Yufeng Zhao for helpful discussion and suggestion of the experiments.

## REFERENCES


(1) Agnoli, S.; Favaro, M. Doping Graphene with Boron: A Review of Synthesis Methods, Physicochemical Characterization, and Emerging Applications. *J. Mater. Chem. A* **2016**, *4*, 5002−5025.

(2) Xu, D.; Chen, W.; Zeng, M.; Xue, H.; Chen, Y.; Sang, X.; Xiao, Y.; Zhang, T.; Unocic, R. R.; Xiao, K.; Fu, L. Crystal-Field Tuning of Photoluminescence in Two-Dimensional Materials with Embedded Lanthanide Ions. *Angew. Chem., Int. Ed.* **2018**, *57*, 755−759.

(3) Peng, Z.; Ye, R.; Mann, J. A.; Zakhidov, D.; Li, Y.; Smalley, P. R.; Lin, J.; Tour, J. M. Flexible Boron-Doped Laser-Induced Graphene Microsupercapacitors. *ACS Nano* **2015**, *9*, 5868−5875.

(4) Ding, Y.; Zeng, M.; Zheng, Q.; Zhang, J.; Xu, D.; Chen, W.; Wang, C.; Chen, S.; Xie, Y.; Ding, Y.; Zheng, S.; Zhao, J.; Gao, P.; Fu, L. Bidirectional and Reversible Tuning of the Interlayer Spacing of Two-Dimensional Materials. *Nat. Commun.* **2021**, *12*, 5886.

(5) Wang, X.; Sun, G.; Routh, P.; Kim, D.-H.; Huang, W.; Chen, P. Heteroatom-Doped Graphene Materials: Syntheses, Properties and Applications. *Chem. Soc. Rev.* **2014**, *43*, 7067−7098.

(6) Wu, G.; McHugh, E. A.; Berka, V.; Chen, W.; Wang, Z.; Beckham, J. L.; Derry, P. J.; Roy, T.; Kent, T. A.; Tour, J. M.; Tsai, A.-L. Oxidized Activated Charcoal Nanoparticles as Catalytic Superoxide Dismutase Mimetics: Evidence for Direct Participation of an Intrinsic Radical. *ACS Appl. Nano Mater.* **2020**, *3*, 6962−6971.

(7) Advincula, P. A.; Luong, D. X.; Chen, W.; Raghuraman, S.; Shahsavari, R.; Tour, J. M. Flash Graphene from Rubber Waste. *Carbon* **2021**, *178*, 649−656.

(8) Lowell, C. E. Solid Solution of Boron in Graphite. *J. Am. Ceram. Soc.* **1967**, *50*, 142−144.

(9) Yu, X.; Han, P.; Wei, Z.; Huang, L.; Gu, Z.; Peng, S.; Ma, J.; Zheng, G. Boron-Doped Graphene for Electrocatalytic $N_2$ Reduction. *Joule* **2018**, *2*, 1610−1622.

(10) Zhang, R.; Chen, X.-R.; Chen, X.; Cheng, X.-B.; Zhang, X.-Q.; Yan, C.; Zhang, Q. Lithiophilic Sites in Doped Graphene Guide Uniform Lithium Nucleation for Dendrite-Free Lithium Metal Anodes. *Angew. Chem., Int. Ed.* **2017**, *56*, 7764−7768.

(11) Han, J.; Cheon, J. Y.; Joo, S. H.; Park, S. Synthesis of Boron and Nitrogen Co-Doped Graphene Nano-Platelets Using a Two-Step Solution Process and Catalytic Properties for Oxygen Reduction Reaction. *Solid State Sci.* **2014**, *33*, 1−5.

(12) Chen, H.; Luo, Q.; Liu, T.; Tai, M.; Lin, J.; Murugadoss, V.; Lin, H.; Wang, J.; Guo, Z.; Wang, N. Boosting Multiple Interfaces by Co-Doped Graphene Quantum Dots for High Efficiency and Durability Perovskite Solar Cells. *ACS Appl. Mater. Interfaces* **2020**, *12*, 13941−13949.

(13) Sheng, Z.-H.; Gao, H.-L.; Bao, W.-J.; Wang, F.-B.; Xia, X.-H. Synthesis of Boron Doped Graphene for Oxygen Reduction Reaction in Fuel Cells. *J. Mater. Chem.* **2012**, *22*, 390−395.

(14) Mu, X.; Yuan, B.; Feng, X.; Qiu, S.; Song, L.; Hu, Y. The Effect of Doped Heteroatoms (Nitrogen, Boron, Phosphorus) On Inhibition Thermal Oxidation of Reduced Graphene Oxide. *RSC Adv.* **2016**, *6*, 105021−105029.

(15) Panchakarla, L. S.; Subrahmanyam, K. S.; Saha, S. K.; Govindaraj, A.; Krishnamurthy, H. R.; Waghmare, U. V.; Rao, C. N. R. Synthesis, Structure, and Properties of Boron- and Nitrogen-Doped Graphene. *Adv. Mater.* **2009**, *21*, 4726−4730.

(16) Tang, Y.-B.; Yin, L.-C.; Yang, Y.; Bo, X.-H.; Cao, Y.-L.; Wang, H.-E.; Zhang, W.-J.; Bello, I.; Lee, S.-T.; Cheng, H.-M.; Lee, C.-S. Tunable Band Gaps and p-Type Transport Properties of Boron-Doped Graphenes by Controllable Ion Doping Using Reactive Microwave Plasma. *ACS Nano* **2012**, *6*, 1970−1978.

(17) Wu, T.; Shen, H.; Sun, L.; Cheng, B.; Liu, B.; Shen, J. Nitrogen and Boron Doped Monolayer Graphene by Chemical Vapor Deposition Using Polystyrene, Urea and Boric Acid. *New J. Chem.* **2012**, *36*, 1385−1391.

(18) Zhou, Z.; Wakamiya, A.; Kushida, T.; Yamaguchi, S. Planarized Triarylboranes: Stabilization by Structural Constraint and Their Plane-to-Bowl Conversion. *J. Am. Chem. Soc.* **2012**, *134*, 4529−4932.

(19) Luong, D. X.; Bets, K. V.; Algozeeb, W. A.; Stanford, M. G.; Kittrell, C.; Chen, W.; Salvatierra, R. V.; Ren, M.; McHugh, E. A.;

Advincula, P. A.; Wang, Z.; Bhatt, M.; Guo, H.; Mancevski, V.; Shahsavari, R.; Yakobson, B. I.; Tour, J. M. Gram-Scale Bottom-Up Flash Graphene Synthesis. *Nature* **2020**, *577*, 647−651.

(20) Chen, W.; Wang, Z.; Bets, K. V.; Luong, D. X.; Ren, M.; Stanford, M. G.; McHugh, E. A.; Algozeeb, W. A.; Guo, H.; Gao, G.; Deng, B.; Chen, J.; Li, J. T.; Carsten, W. T.; Yakobson, B. I.; Tour, J. M. Millisecond Conversion of Metastable 2D Materials by Flash Joule Heating. *ACS Nano* **2021**, *15*, 1282−1290.

(21) Algozeeb, W. A.; Savas, P. E.; Luong, D. X.; Chen, W.; Kittrell, C.; Bhat, M.; Shahsavari, R.; Tour, J. M. Flash Graphene from Plastic Waste. *ACS Nano* **2020**, *14*, 15595−15604.

(22) Yao, Y.; Huang, Z.; Xie, P.; Lacey, S. D.; Jacob, R. J.; Xie, H.; Chen, F.; Nie, A.; Pu, T.; Rehwoldt, M.; Yu, D.; Zachariah, M. R.; Wang, C.; Shahbazian-Yassar, R.; Li, J.; Hu, L. Carbothermal Shock Synthesis of High-Entropy-Alloy Nanoparticles. *Science* **2018**, *359*, 1489−1494.

(23) Li, T.; Pickel, A. D.; Yao, Y.; Chen, Y.; Zeng, Y.; Lacey, S. D.; Li, Y.; Wang, Y.; Dai, J.; Wang, Y.; Yang, B.; Fuhrer, M. S.; Marconnet, A.; Dames, C.; Drew, D. H.; Hu, L. Thermoelectric Properties and Performance of Flexible Reduced Graphene Oxide Films Up To 3,000 K. *Nat. Energy* **2018**, *3*, 148−156.

(24) Chen, W.; Li, J. T.; Wang, Z.; Algozeeb, W. A.; Luong, D. X.; Kittrell, C.; McHugh, E. A.; Advincula, P. A.; Wyss, K. M.; Beckham, J. L.; Stanford, M. G.; Jiang, B.; Tour, J. M. Ultrafast and Controllable Phase Evolution by Flash Joule Heating. *ACS Nano* **2021**, *15*, 11158−11167.

(25) Iglesias, D.; Giuliani, A.; Melchionna, M.; Marchesan, S.; Criado, A.; Nasi, L.; Bevilacqua, M.; Tavagnacco, C.; Vizza, F.; Prato, M.; Fornasiero, P. N-Doped Graphitized Carbon Nanohorns as a Forefront Electrocatalyst in Highly Selective $O_2$ Reduction to $H_2O_2$. *Chem.* **2018**, *4*, 106−123.

(26) Pollard, A. J.; Brennan, B.; Stec, H.; Tyler, B. J.; Seah, M. P.; Gilmore, I. S.; Roy, D. Quantitative Characterization of Defect Size in Graphene Using Raman Spectroscopy. *Appl. Phys. Lett.* **2014**, *105*, 253107.

(27) Jorio, A.; Ferreira, E. H. M.; Moutinho, M. V. O.; Stavale, F.; Achete, C. A.; Capaz, R. B. Measuring Disorder in Graphene with the G and D Bands. *Phys. Status Solidi B* **2010**, *247*, 2980−2982.

(28) Stanford, M. G.; Bets, K. V.; Luong, D. X.; Advincula, P. A.; Chen, W.; Li, J. T.; Wang, Z.; McHugh, E. A.; Algozeeb, W. A.; Yakobson, B. I.; Tour, J. M. Flash Graphene Morphologies. *ACS Nano* **2020**, *14*, 13691−13699.

(29) Tokarczyk, M.; Kowalski, G.; Witowski, A.M.; Kozinski, R.; Librant, K.; Aksienionek, M.; Lipinska, L.; Ciepielewski, P. Structural and Electronic Properties of Graphene Oxide and Reduced Graphene Oxide Papers Prepared by High Pressure and High Temperature Treatment. *Acta Phys. Polym., A* **2014**, *126*, 1190−1194.

(30) Gladkaya, I. S.; Kremkova, G. N.; Slesarev, V. N. Turbostratic Boron Nitride ($BN_t$) Under High Pressure and Temperature. *J. Less-Common Met.* **1986**, *117*, 241−245.

(31) Thomas, J., Jr.; Weston, N. E.; O'Connor, T. E. Turbostratic Boron Nitride, Thermal Transformation to Ordered-layer-lattice Boron Nitride. *J. Am. Chem. Soc.* **1962**, *84*, 4619−4622.

(32) Inagaki, M.; Kang, F. *Materials Science and Engineering of Carbon: Fundamentals*, 2nd ed.; Elsevier Inc., 2014; pp 17−217. DOI: 10.1016/C2013-0-13699-9.

(33) Franklin, R. E. Crystallite Growth in Graphitizing and Non-Graphitizing Carbons. *Proc. R. Soc. London A* **1951**, *209*, 196−218.

(34) Ouzilleau, P.; Gheribi, A. E.; Chartrand, P.; Soucy, G.; Monthioux, M. Why Some Carbons May or May Not Graphitize? The Point of View of Thermodynamics. *Carbon* **2019**, *149*, 419−435.

(35) Nakanishi, K. Porosity Measurement. Handbook of Sol-Gel Science and Technology. *Springer International Publishing AG* **2016**, 1−11.

(36) Radlinski, A. P.; Mastalerz, M.; Hinde, A. L.; Hainbuchner, M.; Rauch, H.; Baron, M.; Lin, J. S.; Fan, L.; Thiyagarajan, P. Application of SAXS and SANS in Evaluation of Porosity, Pore Size Distribution and Surface Area of Coal. *Int. J. Coal Geol.* **2004**, *59*, 245−271.

(37) Chen, W.-T.; Dutta, D.; Hung, Y.-H.; Sin, Y.-Y.; He, S.-M.; Chang, J.-K.; Su, C.-Y. Designed Catalytic Protocol for Enhancing Hydrogen Evolution Reaction Performance of P, N-Co-Doped Graphene: The Correlation of Manipulating the Dopant Allocations and Heteroatomic Structure. *J. Phys. Chem. C* **2020**, *124*, 25701−25711.

(38) Sibul, R.; Põldsepp, E. K.; Mäeorg, U.; Merisalu, M.; Kikas, A.; Kisand, V.; Treshchalov, A.; Sammelselg, V.; Tammeveski, K. Sulphur and Nitrogen Co-Doped Graphene-Based Electrocatalysts for Oxygen Reduction Reaction In Alkaline Medium. *Electrochem. Commun.* **2019**, *109*, 106603.

(39) Wyss, K. M.; Beckham, J. L.; Chen, W.; Luong, D. X.; Hundi, P.; Raghuraman, S.; Shahsavari, R.; Tour, J. M. Converting Plastic Waste Pyrolysis Ash into Flash Graphene. *Carbon* **2021**, *174*, 430−438.

(40) Wang, Z.; Li, Q.-K.; Zhang, C.; Cheng, Z.; Chen, W.; McHugh, E. A.; Carter, R. A.; Yakobson, B. I.; Tour, J. M. Hydrogen Peroxide Generation with 100% Faradaic Efficiency on Metal-Free Carbon Black. *ACS Catal.* **2021**, *11*, 2454−2459.

(41) Wang, L.; Sofer, Z.; Pumera, M. Will Any Crap We Put into Graphene Increase Its Electrocatalytic Effect? *ACS Nano* **2020**, *14*, 21−25.

(42) Ye, R.; Dong, J.; Wang, L.; Cruz, R. M.; Li, Y.; An, P.-F.; Yacaman, M. J.; Yakobson, B. I.; Chen, D.; Tour, J. M. Manganese Deception on Graphene and Implications in Catalysis. *Carbon* **2018**, *132*, 623−631.

(43) Wang, L.; Ambrosi, A.; Pumera, M. "Metal-Free" Catalytic Oxygen Reduction Reaction on Heteroatom-Doped Graphene is Caused by Trace Metal Impurities. *Angew. Chem., Int. Ed.* **2013**, *52*, 13818−13821.

(44) Chen, W.; Salvatierra, R. V.; Ren, M.; Chen, J.; Stanford, M. G.; Tour, J. M. Laser-Induced Silicon Oxide for Anode-Free Lithium Metal Batteries. *Adv. Mater.* **2020**, *32*, 2002850.

(45) Salvatierra, R. V.; Chen, W.; Tour, J. M. What Can be Expected from "Anode-Free" Lithium Metal Batteries? *Adv. Energy Sustainability Res.* **2021**, *2*, 2000110.

(46) For scaleup of FJH for graphene synthesis, see: https://www.universalmatter.com/ (accessed December 8, 2021).



https://doi.org/10.1021/acsnano.2c01136
*ACS Nano* XXXX, XXX, XXX−XXX